Geosphere

Previously unrecognized regional structure of the Coastal Belt of the Franciscan Complex, northern California, revealed by magnetic data

V.E. Langenheim, R.C. Jachens, C.M. Wentworth and R.J. McLaughlin

Geosphere published online 11 October 2013;
doi: 10.1130/GES00942.1

Notes

Previously unrecognized regional structure of the Coastal Belt of the Franciscan Complex, northern California, revealed by magnetic data

V.E. Langenheim, R.C. Jachens, C.M. Wentworth, and R.J. McLaughlin
U.S. Geological Survey, 345 Middlefield Road, Menlo Park, California 94025, USA

ABSTRACT

Magnetic anomalies provide surprising structural detail within the previously undivided Coastal Belt, the westernmost, youngest, and least-metamorphosed part of the Franciscan Complex of northern California. Although the Coastal Belt consists almost entirely of arkosic graywacke and shale of mainly Eocene age, new detailed aeromagnetic data show that it is pervasively marked by long, narrow, and regularly spaced anomalies. These anomalies arise from relatively simple tabular bodies composed principally of magnetic basalt or graywacke confined mainly to the top couple of kilometers, even though metamorphic grade indicates that these rocks have been more deeply buried, at depths of 5–8 km. If true, this implies surprisingly uniform uplift of these rocks. The basalt (and associated Cretaceous limestone) occurs largely in the northern part of the Coastal Belt; the graywacke is recognized only in the southern Coastal Belt and is magnetic because it contains andesitic grains. The magnetic grains were not derived from the basalt, and thus require a separate source. The anomalies define simple patterns that can be related to folding and faulting within the Coastal Belt. This apparent simplicity belies complex structure mapped at outcrop scale, which can be explained if the relatively simple tabular bodies are internally deformed, fault-bounded slabs. One mechanism that can explain the widespread lateral extent of the thin layers of basalt is peeling up of the uppermost part of the oceanic crust into the accretionary prism, controlled by porosity and permeability contrasts caused by alteration in the upper part of the subducting slab. It is not clear, however, how this mechanism might generate fault-bounded layers containing magnetic graywacke. We propose that structural domains defined by anomaly trend, wavelength, and source reflect imbrication and folding during the accretion process and local plate interactions as the Mendocino triple junction migrated north, a hypothesis that should be tested by more detailed structural studies.

INTRODUCTION

Rocks of the Coastal Belt of the Franciscan Complex in the northern California Coast Ranges have proved strikingly resistant to geologic subdivision since the belt was first delineated by W.P. Irwin more than 50 yr ago (Irwin, 1960). He recognized the Coastal Belt as the western of three northwest-trending belts in the northern Coast Ranges that comprise what is now called the Franciscan Complex (Fig. 1), long considered a classic example of a subduction-generated accretionary prism that records progressive accretion to the North American continental margin since the Jurassic. The older rocks of the blueschist-grade Eastern Belt and mélange-rich Central Belt have since been subdivided into various distinctive units and terranes, but the Coastal Belt has been subdivided only in its northwestern part. Otherwise, it has been mostly depicted as a vast, monotonous terrain of low-grade, arkosic metagraywacke and argillite, with relatively flat isostatic gravity (Roberts et al., 1990) and magnetic signatures (Roberts and Jachens, 1999).

It is with surprise, therefore, that we find considerable detail and coherence expressed through much of the Coastal Belt in recently acquired, high-resolution aeromagnetic data (Langenheim et al., 2011). Aeromagnetic data have been used to map large, regional crustal structures, such as crystalline basement, in subduction zones (Grantz et al., 1963; Finn, 1990); only in the past decade or two have advances in measurement and navigation technology, data processing, and interpretational methods made it possible to investigate structures such as faults and folds within the overlying sedimentary sequence in settings such as the forearc (Saltus et al., 2005). Our study is the first that we know of that maps and analyzes shallow structure within an accretionary prism using detailed aeromagnetic data. The detailed aeromagnetic data reveal that much of the Coastal Belt proves to be marked by long, narrow, regularly spaced magnetic anomalies that define simple patterns (Fig. 1, inset; Fig. 2). Here we build upon work by Phelps et al. (2008a, 2008b) and Langenheim et al. (2011) by using existing information supplemented by several reconnaissance traverses across the Coastal Belt carried out after the new aeromagnetic coverage was obtained. We explore the sources of these anomalies and their implications for structural interpretation of the Coastal Belt.

COASTAL BELT

The Coastal Belt is the westernmost part of the Franciscan Complex, which recorded the continental accretion at a convergent margin from Late Jurassic to Miocene time (Blake et al., 1988; Dumitru et al., 2010; Ernst, 2011; McLaughlin et al., 2000). The overall style of the complex is eastward underthrusting of progressively lower-grade and generally younger rocks, with the Coastal Belt thrust marking the suture between the Coastal and Central Belts, much modified by younger faults and folds in its southernmost part (Fig. 1). The Coastal Belt itself covers an area of ~5500 km^2 and consists almost entirely of potassium-feldspar–bearing arkosic graywacke and shale with abundant laumontite veins (Bailey et al., 1964). It is folded at outcrop scale, and deformation extends from typical broken formation to more severely sheared rock and mélange. Aside from Miocene rocks mapped near the Mendocino triple junction as part of the King Range and False Cape terranes (McLaughlin et al., 1982; Aalto et al., 1995), the Coastal Belt is now thought to be almost entirely of Eocene age (Evitt and Pierce, 1975; Dumitru et al., 2013), except for local, small masses of basaltic volcanics with associated latest Cretaceous foraminiferal limestones that form the depositional basement for the overlying graywacke. Those masses have been interpreted to represent oce-

Geosphere; December 2013; v. 9; no. 6; doi:10.1130/GES00942.1; 9 figures; 1 table.
Received 26 April 2013 ♦ Revision received 12 August 2013 ♦ Accepted 29 August 2013 ♦ Published online 11 October 2013

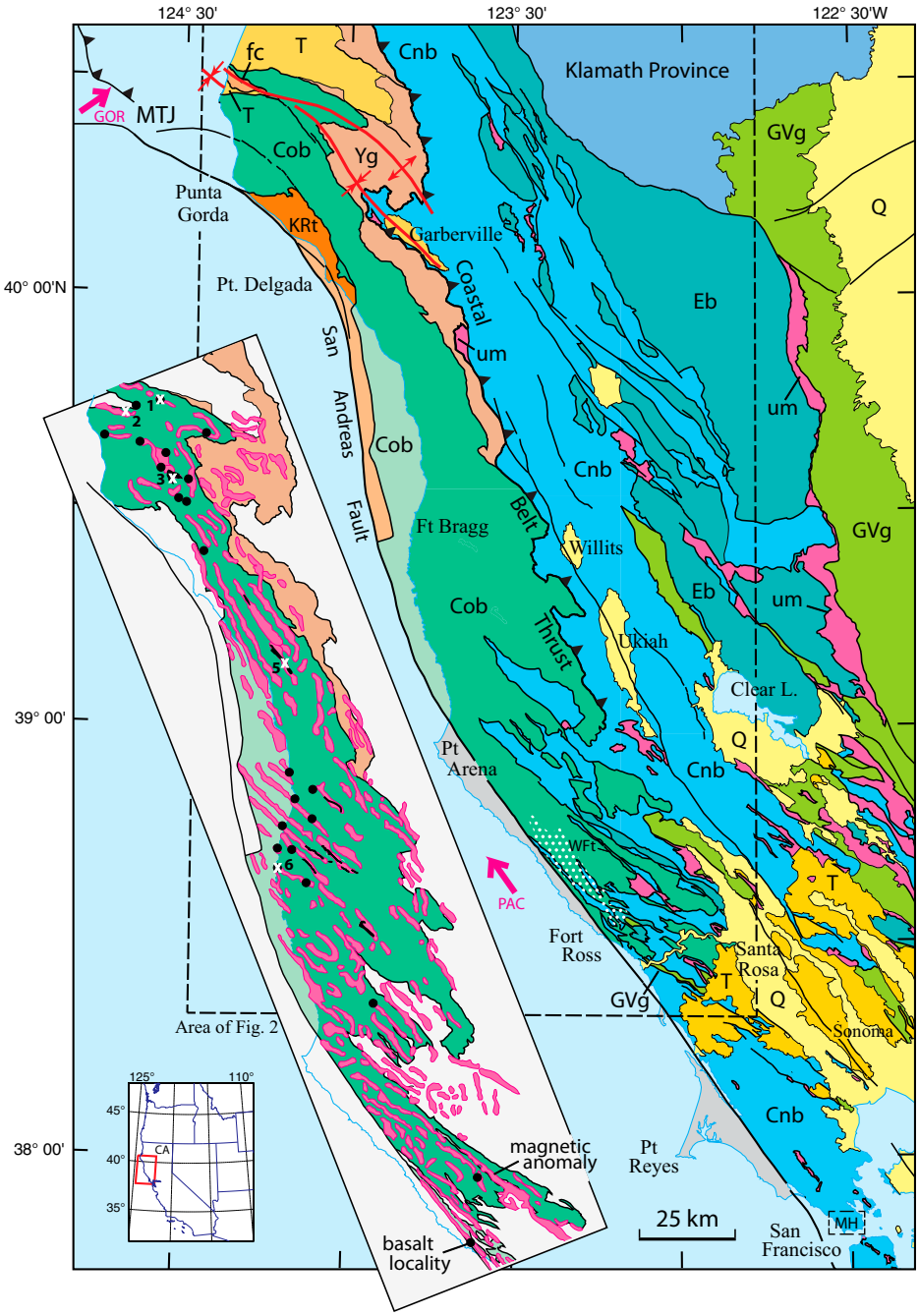

Figure 1. Map showing location and geologic setting of the Franciscan Coastal Belt in the northern California Coast Ranges. Inset shows magnetic anomalies (in magenta) of Figure 2 in and near the Coastal Belt, mapped occurrences of basalt (black dots and areas), and associated fossil localities (numbered white X's; listed in Table 1). Map units: fc—Franciscan False Cape terrane; KRt—Franciscan King Range terrane; Cob—Franciscan Coastal Belt, undivided; Yg—Franciscan Yager terrane; Cnb—Franciscan Central Belt; Eb—Franciscan Eastern Belt; um—ultramafic rocks; MTJ—Mendocino triple junction; GVg—Great Valley Group; T—Tertiary cover; Q—alluvium, largely Quaternary. Stippled pattern near Fort Ross shows outcrop of Ohlson Ranch Formation. Magenta arrows labeled PAC and GOR show relative plate motion of Pacific and Gorda plates, respectively, relative to the North American plate (McCrory, 2000). Tiny box labeled MH—Marin Headlands (area of Fig. 8). Coastal Belt thrust is shown with thrust teeth. Geology was compiled and simplified from Jennings (1977), Blake et al. (1992), Blake et al. (2002), Jayko et al. (1989), McLaughlin et al. (2000), U.S. Geological Survey and California Geological Survey (2006), and geologic mapping by R.J. McLaughlin northeast of Clear Lake and south of Willits. Southern part of the Coastal Belt thrust west and south of Willits is from (1) mapping by McLaughlin, interpretation of aeromagnetic anomalies, and 1:62,500 scale topography, and (2) that east of Point Arena is from photogeologic interpretation that resulted in a greater extent of mélange assigned to the Central Belt.

anic fragments that originated at northern equatorial latitudes (Sliter, 1984; Sliter et al., 1986; McLaughlin et al., 1994, 2000), which were covered by arc and continental sediments as they approached the subduction margin. In a few places, near Fort Bragg and Dugans Opening (locality 5 in Fig. 1 inset), basalt is mapped as elongate bodies (O'Day, 1974; Kramer, 1976). The outcrops of the basalt are generalized from their mapping of fold axes based on bedding and shear attitudes and the discontinuous and irregular distribution of definite volcanic outcrops that may be as much as 1 km apart.

Mapping in the Coastal Belt south from the Mendocino triple junction (McLaughlin et al., 2000; Jayko et al., 1989; Underwood and Bachman, 1986) has distinguished some younger outboard elements near the coast (mid-Miocene King Range and False Cape terranes) and the less severely deformed Yager terrane to the east, but the remainder, called the Coastal terrane, represents the northwestern continuation of the great mass of undivided Coastal Belt to the south. The Yager terrane (originally Yager Formation of Ogle, 1953), of Eocene age, extends southward along the eastern side of the Coastal Belt, where it is distinguished from the Coastal terrane principally by its typically less severe internal deformation, less abundant laumontite veining, and absence of volcanics. It lies in apparent thrust contact with the underlying and more westerly Coastal terrane.

Farther to the south, a narrow fault slice along the eastern margin of the Coastal Belt attributed to the Wheatfield Fork terrane (WFt in Figs. 1 and 2) is distinguished by the Eocene age of both limestone associated with mafic volcanics and of the overlying graywacke (McLaughlin et al., 2009; Blake et al., 2002). Cretaceous lime-

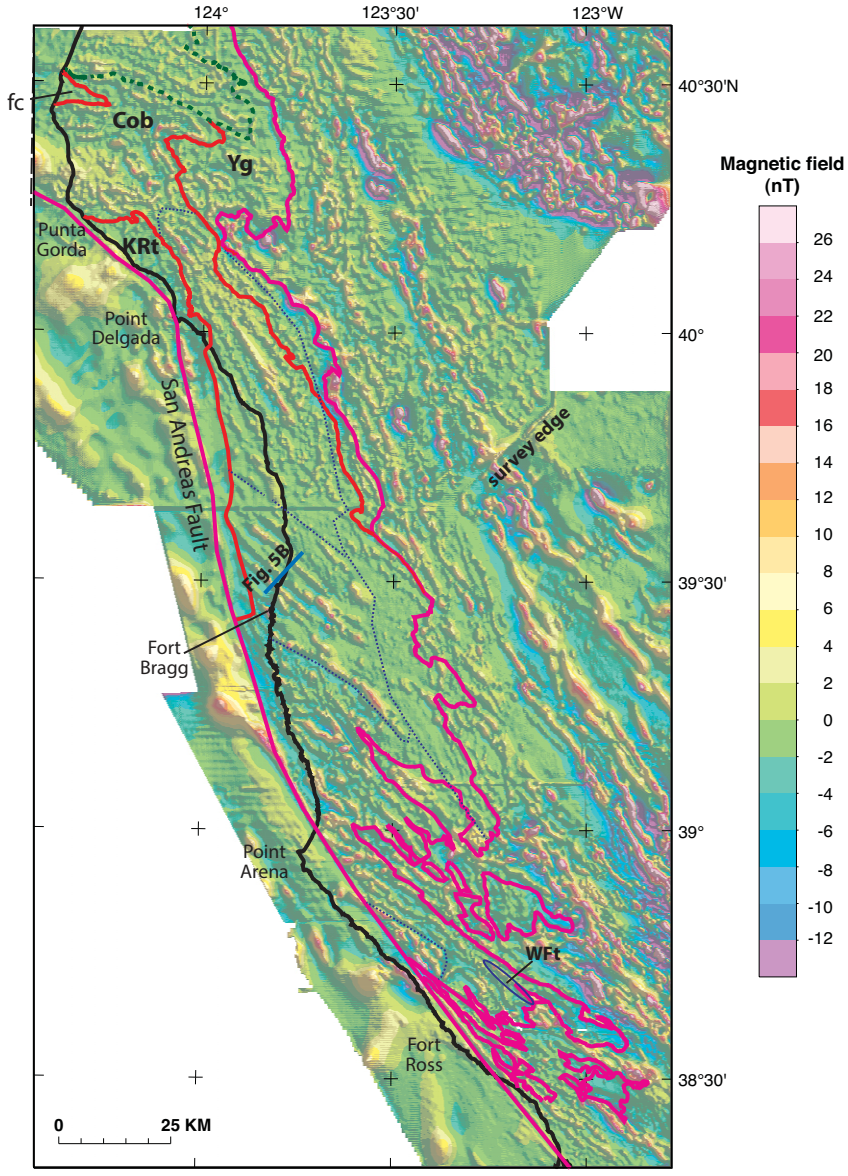

Figure 2. Filtered magnetic map of the Coastal Belt. See Langenheim et al. (2011) for details of filtering that places anomalies over magnetic sources and enhances anomalies for which sources are exposed or near surface. Magenta lines—margins of the belt, with the San Andreas fault on the west and the Coastal Belt thrust and other faults on the east. Dashed dark green lines—depositional contacts. Red lines—boundaries between the terranes of the Coastal Belt: Coastal Belt, undivided (Cob), False Cape terrane (fc), King Range terrane (KRt), and Yager terrane (Yg). The Wheatfield Fork terrane (WFt) is too narrow to show at the scale of the figure, but its extent along the eastern boundary of the Coastal Belt is circled in dark blue. Thin dark blue dotted lines separate structural domains discussed in text and shown in figure 6. Blue line—profile location of model shown in Figure 5B.

stone and basalt are also present in the lower part of the Wheatfield Fork terrane volcanic section. Eocene volcanics are not otherwise known within the Coastal Belt, which is characterized by Late Cretaceous limestone associated with the mafic volcanics.

In contrast to the Coastal Belt, the Central Belt consists predominantly of mélange that encloses large blocks and slabs of various Franciscan rock types of Jurassic to Late Cretaceous age (Murchey and Jones, 1984; Blake et al., 1988). Blocks and slabs include classic rock types associated with the Franciscan Complex such as radiolarian chert, metabasalt, blueschist, eclogite, amphibolite, and serpentinite. The western margin of the Central Belt is marked by discontinuous lenses and masses of ophiolitic rocks at the structural base of the Central Belt (McLaughlin et al., 1988, 1994, 2000; Ernst and McLaughlin, 2012). This contact is relatively straight to mildly folded along most of its length. Near the southern end of the Coastal Belt, long tongues of Central Belt extend northwestward into the Coastal Belt to define faulted folds in the basal thrust, a structural style that is expressed throughout the Coastal Belt to the north.

MAGNETIC INFORMATION

The foundation of our analysis of the Coastal Belt structure consists of newly merged, detailed aeromagnetic data (Langenheim et al., 2011). The data were collected during the past 20 yr in six separate surveys conducted from low-flying aircraft (≤300 m nominal height above ground) along flight lines spaced 450–800 m apart. Flight lines were flown perpendicular to the dominant structural strike. The data were placed on a common magnetic datum and merged to provide an areally continuous and detailed aeromagnetic data set that covers the entire extent of the Coastal Belt. Procedures that are discussed in detail by Langenheim et al. (2011) were then applied (1) to center the magnetic highs over the magnetic source bodies and (2) to enhance those anomalies produced by exposed or near-surface magnetic bodies (see Fig. 2).

The new data reveal a magnetic grain that was not evident in the earlier, far less detailed coverage. Long, narrow, linear-to-curvilinear magnetic anomalies characterize much of the Coastal Belt, with noticeable exceptions in the King Range and False Cape terranes, where the magnetic field is smooth with generally lower values (Fig. 2). The Coastal Belt anomalies are generally of low amplitude (2–20 nT), with anomaly widths of ~1 km and lengths of 10–40 km. In places, particularly in the western part of the Coastal Belt, the anomalies have a characteristic and regular spacing of 2–4 km. The anomaly trend is generally north-northwest to west-northwest. The magnetic anomaly patterns imply a surprising degree of regularity, coherence, and spatial continuity within much of the Coastal Belt, which contrasts sharply with the structural complexity observed at outcrop scale in many areas (e.g., McLaughlin et al., 1994; Fig. 3).

MAGNETIC ANOMALY SOURCES

Magnetic anomalies are caused by the presence of magnetic minerals, principally mag-

Figure 3. Photo near the eastern margin of the Coastal terrane (at Cathey's Peak, latitude 40°16.405′N, longitude 124°4.670′W). Here, interbedded sandstone and argillite are complexly folded, with sheared and detached anticlinal hinges. Sandstones in the exposure are extensively fractured and veined with laumontite.

netite. Anomalies can often be related to rock type by comparing the magnetic anomaly map with available geologic maps and by measuring the magnetic susceptibility of rock samples and outcrops. The three main sources for the magnetic anomalies in and along the margins of the Coastal Belt are (1) ultramafic and gabbroic (ophiolitic) rocks that have been correlated with the Jurassic Coast Ranges ophiolite and are limited to the eastern margin of the Coastal Belt, (2) mafic volcanic rocks that are latest Cretaceous in age, and (3) Tertiary lithic graywacke.

Ophiolite

The most obvious sources of magnetic anomalies in all of the Franciscan Complex are ophiolitic rock types (serpentinite, serpentinized peridotite, and gabbro), which are very magnetic (Saad, 1969) and are well known as magnetic sources in northern and central California. Fragments of Jurassic Coast Range ophiolite, including many serpentinite bodies, occur at the western margin of the Central Belt along the northern part of the Coastal Belt thrust (McLaughlin et al., 1988, 2000; Jayko et al., 1989) and are likely farther south as well, based on available geologic mapping and the distribution of magnetic anomalies. Within the Coastal Belt itself, however, such rocks are almost completely absent and are not the source of the Coastal Belt magnetic anomalies.

Mafic Volcanic Rock in the Coastal Belt

Mafic volcanic rocks, which also can be very magnetic, have been documented at scattered localities in the Coastal Belt (Fig. 1, inset; Table 1). Where measured, these rocks exhibit high magnetic susceptibilities ($\geq 10^{-2}$ SI units), as detailed in Langenheim et al. (2011). The volcanic localities are located principally across the northern two thirds of the Coastal Belt, although a handful of outcrops have been documented to the south. Most volcanic localities are spatially coincident with the magnetic anomalies. The anomalies may provide previously unrecognized spatial coherence to these scattered outcrops.

Where studied, the basalts consist of pillowed flows and flow breccia (locally interbedded with argillite and tuff) and isolated diabase dikes and sills that are tholeiitic to alkalic in composition (McLaughlin et al., 1994). Hornblende is absent, as would be expected for basalt of this composition. These rocks are considered to be accreted fragments of oceanic basalt (McLaughlin et al., 1994; Sliter et al., 1986) that have not been sufficiently metamorphosed or hydrother-

TABLE 1. AGES OF FOSSILS FROM LIMESTONE ASSOCIATED WITH BASALTS

Map no.	Long (°W)	Lat (°N)	Locality	Age	Paleontologic criteria	Source/reference
1	124.1844	40.47339	Hacketsville	Middle Maastrichtian	Planktic foraminifers (*Gansserina ganserri* zone, 71–69 Ma)	Sliter et al. (1986)
2a	124.2938	40.44961	Bear River	Late Campanian	Planktic foraminifers (*Globotruncana ventricosa* zone, 78–75 Ma)	Sliter et al. (1986)
2b	124.2867	40.44721	Bear River	Late Campanian	Planktic foraminifers (*Globotruncana ventricosa* zone, 78–75 Ma)	Sliter et al. (1986)
3	124.1448	40.29319	Parkhurst Ridge	Early Campanian to early Maastrichtian	Planktic foraminifers (*Globotruncanita elevata* zone to at least *Globotruncana falsostuarti* zone, 82–72 Ma)	Sliter et al. (1986)
4	124.0466	40.07269	Queen Peak (King Range terrane)	Middle Miocene	Radiolaria (*Certocapsella tetrapera* and *Stichocorys* sp., est. ca. 15–18 Ma)	S.A. Kling *in* McLaughlin et al. (1982)
5	123.7985	39.86877	Dugans Opening	Campanian and early Maastrichtian	Planktic foraminifers (in part *Globotruncanella havanensis* zone, ca. 74 Ma)	McLaughlin et al. (1994)
6	123.8136	39.39219	Mitchell Creek	Campanian to Maastrichtian	Planktic foraminifers	W.V. Sliter (1987, personal commun.)
7	123.25	38.73079	Wheatfield Fork terrane	Middle Eocene	Planktic foraminifers (late Ulatisian–Narizian, P-11 to P-14; CP 13–14; ca. 41–49 Ma)	W.V. Sliter laboratory notes, from McLaughlin (paper in prep)

Note: See Figure 1: note that localities 4 and 7 are not shown on the figure.

mally altered to destroy magnetite (in contrast to the weakly magnetic greenstone in most of the Central Belt). Although the basalts are too altered for radiometric dating, in a few scattered places (Fig. 1, inset), they are depositionally intercalated with or overlain by pelagic limestones that have yielded foraminifera of northern equatorial affinity, all of latest Cretaceous age (Sliter, 1984; Sliter et al., 1986; Table 1). In some cases, the depositional contact has been subsequently sheared.

A long, linear body that also produces a magnetic anomaly is Eocene and Cretaceous basalt in the Wheatfield Fork terrane (Blake et al., 2002; McLaughlin et al., 2009), located near the south end of the Coastal Belt. As noted earlier, this basalt is the only known occurrence of Eocene volcanic rock within the Coastal Belt.

Lithic Graywacke in the Coastal Belt

A third, unexpected source for some of the magnetic anomalies in the Coastal Belt is graywacke containing volcanic lithic grains. Most sedimentary rocks are only weakly magnetic, and, to our knowledge, nowhere else in the Franciscan Complex are magnetic anomalies associated with graywacke. The small subset of sedimentary rocks that produce measurable magnetic anomalies includes those containing volcanic lithic grains. Well-known examples elsewhere in California of sandstones that are magnetic because of volcanic lithic grains include the Neroly Formation east of San Francisco, parts of the Purisima Formation in the Santa Cruz Mountains (Hillhouse and Jachens, 2005), Cretaceous turbidites in southern California (Langenheim et al., 2006), and sandstones of the Great Valley Group (Langenheim et al., 2010). Reconnaissance measurements of magnetic susceptibility along roads south of Fort Bragg (Phelps et al., 2008a, 2008b; Langenheim et al., 2011) indicate that some graywacke within the magnetic anomalies is magnetic, with susceptibilities of 2–30 × 10^{-3} SI units. Other graywacke, both within and outside the magnetic anomalies, has susceptibilities less than 1 × 10^{-3}, and in most cases less than 0.25 × 10^{-3} SI units. The magnetic graywacke could be a subset of the lithic graywacke petrofacies identified within the Coastal terrane by Jayko and Blake (1984) and Underwood and Bachman (1986), although it is not clear if their lithic graywacke is magnetic or corresponds with magnetic anomalies. Their classification is based on petrographic analysis and has not been used for mapping subunits within the Coastal Belt. Magnetic anomalies in the Yager terrane north of Garberville are likely related to conglomerate and sandstone, a conclusion supported by a handful of magnetic susceptibility measurements reported by Langenheim et al. (2011).

Three graywacke samples from our reconnaissance were selected for additional analysis to determine the source of the magnetic susceptibility. The samples were ground to a fine powder in a porcelain mortar and tested with a hand magnet. One sample, with a magnetic susceptibility of 10^{-2} SI units, yielded conspicuous fine magnetite, whereas the other two samples, with magnetic susceptibilities of <0.3 × 10^{-3} SI units, yielded only trace to no magnetite.

Thin sections of a different, dark-green lithic graywacke, located within a magnetic anomaly and having a magnetic susceptibility of 1.0–1.7 × 10^{-2} SI units, revealed common equant opaque grains (<1 mm), likely magnetite, both as individual detrital grains and as grains within volcanic rock fragments (Fig. 4). Lithic fragments in the thin sections are largely basaltic to andesitic volcanic clasts, with plagioclase both as intersertal laths and as zoned and twinned phenocrysts enclosed by a glassy intersertal to hyalophitic or intergranular matrix. Detrital potassium feldspar is a minor constituent (3%) of the sandstone and is in somewhat less abundance than in the majority of Coastal Belt graywacke, which contains as much as 20% potassium feldspar (Bailey et al., 1964; Underwood and Bachman, 1986). Potassium feldspar also occurs in some of the intermediate volcanic clasts. Of particular note is the presence of clasts of porphyritic hornblende andesite that include distinctive blue-green amphibole intergrown with subhedral plagioclase (Fig. 4). Primary hornblende and potassium feldspar in the andesitic clasts suggest that the volcanic material is arc-derived, and this contrasts strongly with the ocean-floor affinity of the alkali to tholeiitic basalt flows observed in the Coastal Belt. This contrast in composition indicates that the volcanic clasts in the lithic sandstones cannot have been derived from the basalt in the Coastal Belt.

GEOMETRY OF MAGNETIC SOURCES

The curvilinear magnetic anomalies indicate the presence of magnetic source rocks, but the anomalies also provide information about the three-dimensional shape and continuity of those sources. The horizontal continuity of the anomalies indicates equivalent continuity of the sources in a background of weakly to nonmagnetic rocks, while the shapes of cross-sectional profiles of the anomalies indicate that the sources are tabular bodies and that their dips range from vertical to gently inclined (discussed in the following sections).

The shape of the magnetic anomaly profile across a thin (compared to the measurement height), tabular, dipping magnetic layer varies with dip such that the dip can be estimated (Fig. 5A). For anomalies processed as in this report, a vertical thin layer produces a prominent magnetic high centered over the layer flanked by identical magnetic lows. With decreasing dip, the flanking lows become progressively more asymmetric, with the updip low deepening and the downdip low shallowing. As the dip flattens (for a layer with finite downdip length), a distinct anomaly associated with the downdip edge becomes measurable, and ultimately, for a flat-lying layer, mirror-image high-low anomalies appear over both edges, with the lows posi-

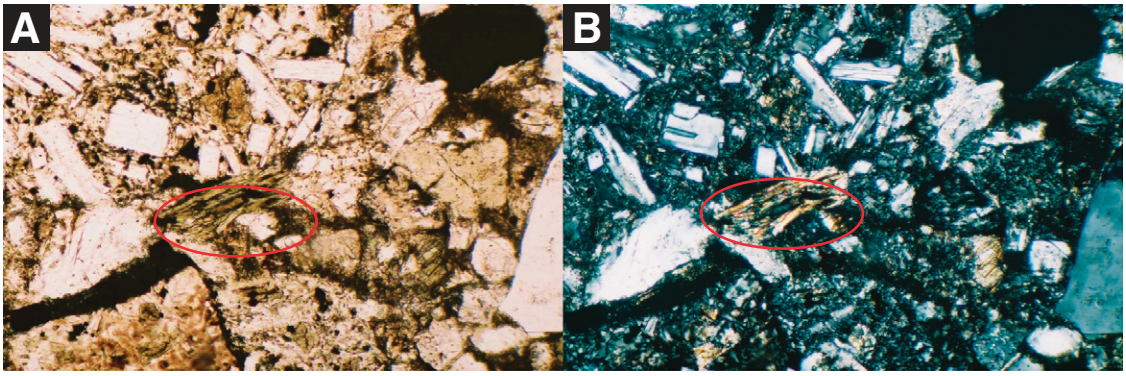

Figure 4. Photomicrographs of magnetic lithic-rich graywacke under (A) normal light and (B) polarized light. Note angular andesitic clasts, including hornblende (red circle) within an altered porphyritic plagioclase-rich volcanic clast. Finely dispersed opaque grains likely are magnetite. Width of field is 0.75 mm.

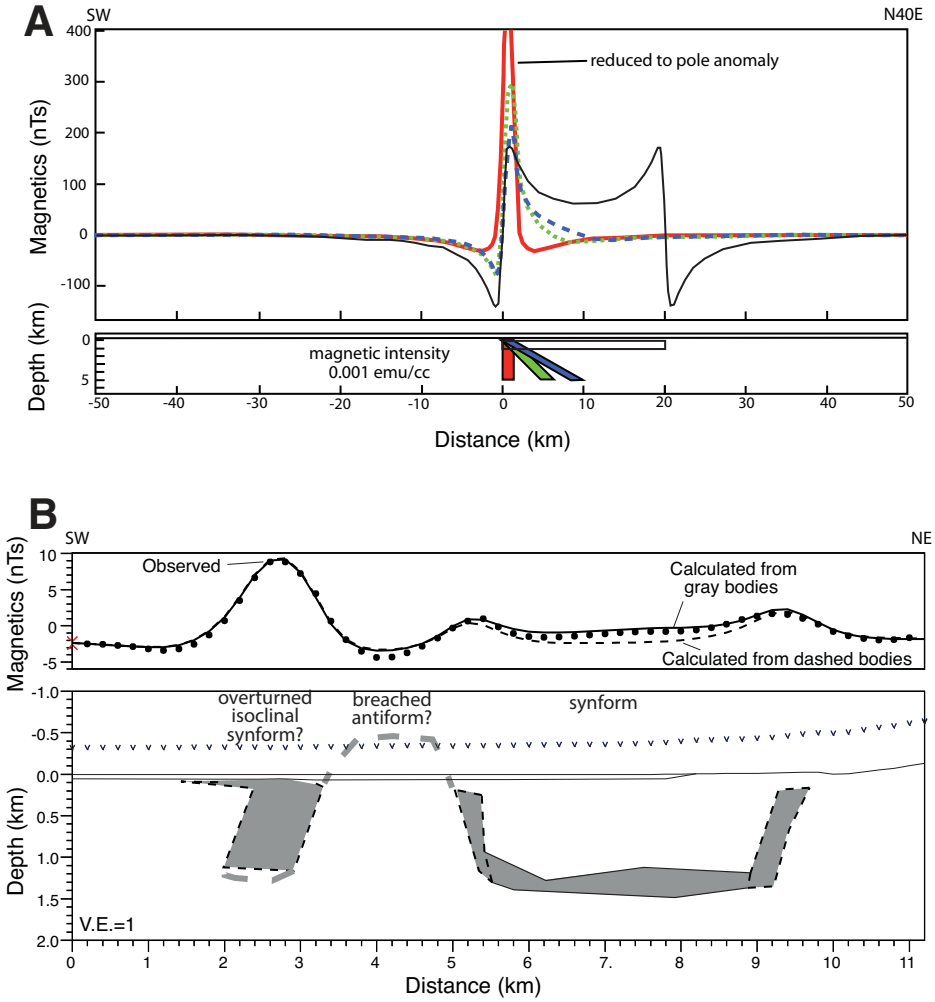

Figure 5. (A) Forward magnetic models that show the effect of dip on anomaly shape and symmetry. Horizontal layers produce prominent magnetic high-low pairs at the edges of the layer, whereas vertical layers produce symmetric magnetic lows bounding a single magnetic high. For a northeast-dipping layer, the amplitude of the low southwest of the high increases relative to the amplitude of the high and relative to the low on the northeast side of the high. (B) Model across magnetic basalt. See Figure 2 for profile location. Observed filtered magnetic anomaly is fit better with a single folded layer (gray body on right) than with separate, isolated magnetic bodies (dashed outlines). Magnetic susceptibility values are 10^{-3} SI units. Small v's in cross section denote location of magnetometer above the ground. Location of inferred breached antiform is consistent with northwest projection of the Indian Springs anticline of Kramer (1976) on line of section. The southwest limb is thicker because of folding, as suggested by the bifurcation of the associated magnetic anomaly to the southeast; alternatively, the thicker limb may result from faulting or thickness variations of the magnetic layer.

tioned outboard of the source body. Another way of viewing the anomaly over a thin vertical layer is that it simply is the anomaly over a flat-lying layer of finite vertical thickness, the lateral edges of which are so close together that the two "edge" anomaly highs merge into a single high.

Magnetic anomalies from folded magnetic sheets that are not truncated at the topographic surface can appear similar to those described here. A magnetic sheet folded into a symmetrical antiform with a vertical axial plane will produce a symmetrical magnetic high similar to that over the vertical sheet described here, although the amplitudes and widths of the high and flanking lows will be somewhat greater. Similarly, an overturned buried folded magnetic sheet will produce an asymmetrical anomaly similar to that over a dipping layer.

The asymmetry of the flanking lows for a dipping magnetic layer indicates (1) that the magnetic sources are layers rather than rods, and it indicates (2) the direction of dip for the layer. Magnetic anomalies produced from subhorizontal rods are necessarily symmetrical, whereas many of the Coastal Belt anomalies are asymmetric. We conclude that the sources of the magnetic anomalies are, in fact, tabular magnetic layers, and we use the degree of anomaly asymmetry of the filtered magnetic data of Figure 2 to determine both dip direction and approximate dip angle for many of the layers (Fig. 6) (subject to the caveats discussed by Langenheim et al., 2011).

The widths of the linear anomalies, and by implication, the thicknesses of their source layers, are remarkably uniform throughout the entire Coastal Belt. The processing applied to the magnetic data produced automatically determined estimates of the boundary locations of the magnetic source bodies (see Langenheim et al., 2011), and these provided a consistent basis for measuring anomaly width. Fifty to one-hundred widths measured in each of four roughly equal areas subdividing the Coastal Belt from north to south yielded median widths of 1.0, 1.1, 1.0, and 1.1 km, with an overall mean of 1.1 ± 0.28 km (±1 standard deviation; $n = 248$). The actual layer thicknesses of the magnetic graywacke or basalt are somewhat less, probably a few hundred to a measured 700 m, because (1) the magnetic field was measured at a height of ~300 m above the ground and (2) nonvertical layers appear thicker in plan view than they actually are. Anomaly widths are exaggerated relative to actual body widths by about the height of the aircraft above the ground (~300 m for this study), because of the smoothing effect of measuring the magnetic field at a distance from the source (Grauch and Cordell, 1987). This effect was illustrated at Laguna Point, just north of Fort Bragg, by comparing an aeromagnetic profile with one measured at ground level (fig. 8 *in* Langenheim et al., 2011). The width defined there from the airborne data is slightly less than 1 km, whereas that defined from the ground data is considerably less (200–300 m). The exaggerated apparent widths amount to a factor of ~1.5–2 for moderate to low dips.

The processing and filtering that produced the magnetic field shown in Figure 2 enhanced the anomalies from near-surface sources at the expense of anomalies from deeper sources (Langenheim et al., 2011). Anomalies in the original magnetic data with wavelengths greater than ~4 km (crudely equivalent to anomalies from sources more than 2 km deep) were attenuated by more than 70%, ensuring that the anomalies we analyze here are caused by sources in the top few kilometers of the crust. These are the sources that should be most closely associated with the surface geology.

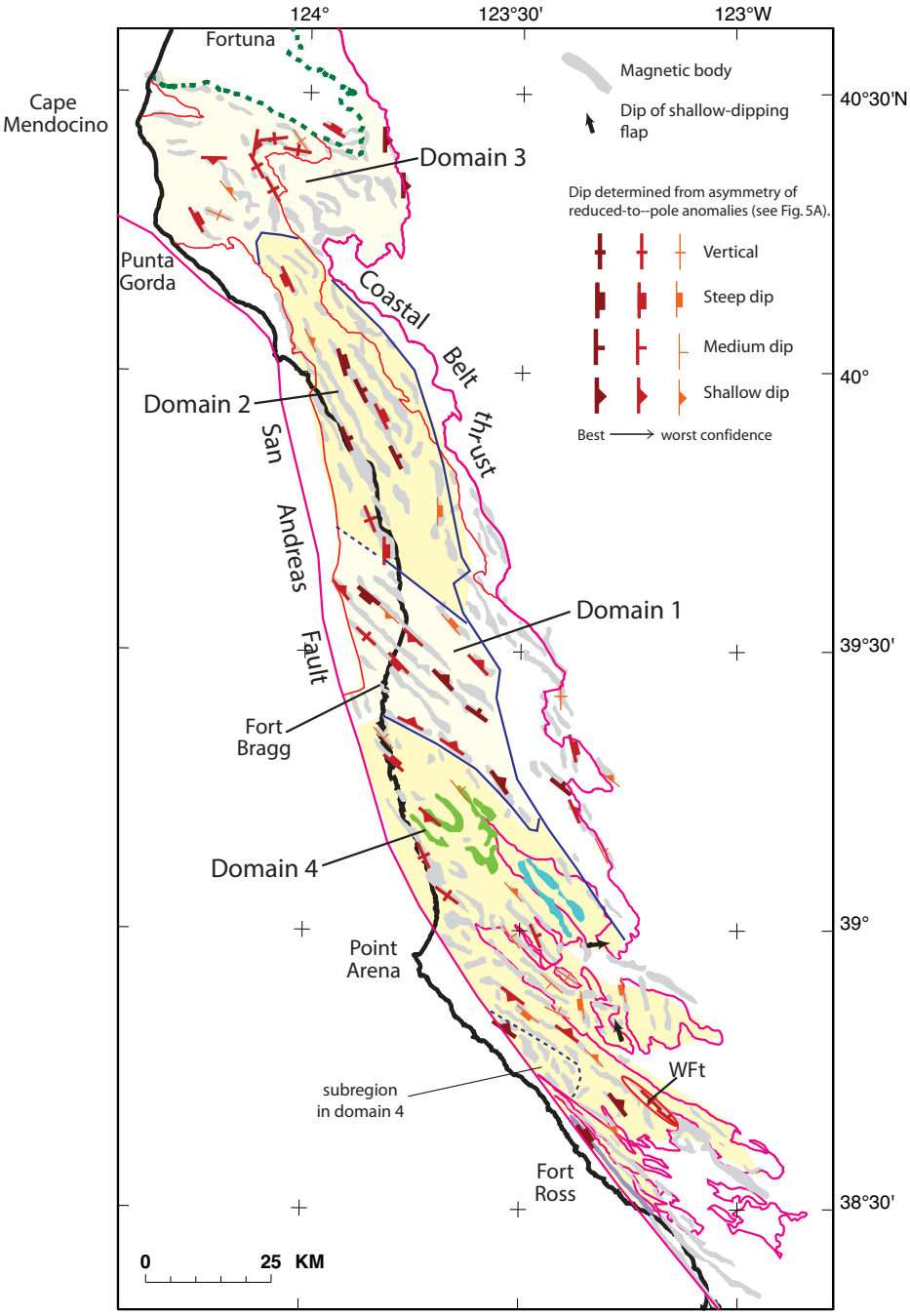

Figure 6. Structural domains and dips interpreted from filtered magnetic anomalies (Fig. 2). Layer dip from asymmetry of magnetic anomaly is shown. Dark blue lines separate domains discussed in text. Anomalies within area east of the Coastal Belt thrust may be caused by magnetic layers in the Coastal Belt beneath a thin sheet of Central Belt rocks in the hanging wall of the thrust. Anomalies colored green, blue, and lavender are discussed in text. WFt—Wheatfield Fork terrane. Dashed green line is outline of onshore Eel River basin.

We examined the original magnetic data to determine if we could detect anomaly patterns from magnetic sources deeper than 2 km comparable to the long, narrow, curvilinear anomalies that dominate Figure 2. The results showed that (1) magnetic sources are present at depths greater than 2 km, some of which seem to connect with the shallow sources, but (2) we were unable to detect the strikingly regular patterns that dominate Figure 2. Some of this failure undoubtedly results from the natural attenuation of short-wavelength anomalies with increasing depth, but at least in the Fort Bragg area, these deeper sources do not seem to mimic the geometry of the shallower sources. This implies that most of the magnetic sources of the anomalies in Figure 2 do not extend more than ~2 km below the ground surface, with the caveat that some of the narrow or thin sources may not be resolvable at depths of more than 2 km.

Architecture of Magnetic Layers

We conclude that the magnetic anomalies in the Coastal Belt are produced by magnetic layers that contain magnetic basalt and/or magnetic graywacke, with layer thickness in the range of a few hundred to 700 m. We use the word layer here in a geometric, rather than a stratigraphic, sense. Stratigraphic organization in these rocks is an entirely separate issue, as discussed later herein.

The internal structure of the magnetic units as individual layers is not as simple as the patterns of the magnetic anomalies would suggest. We have identified magnetic basalts (predominantly in the north) and magnetic graywackes (in the south) as the sources of the Coastal Belt magnetic anomalies, but we further note that the magnetic layers are not composed solely of these rocks. Instead, the magnetic rocks are intermixed with nonmagnetic rocks, and their interrelations seem more structural than stratigraphic. Most of the rocks are at least sheared and typical of a broken formation, and at outcrop scale, the rocks exhibit folds and fault-separated domains having different attitudes of bedding and degrees of shearing. The magnetic layers are thus not stratigraphic layers, but structural layers, and their boundaries must in themselves be faults, thereby reconciling the internal deformation of the magnetic layers at outcrop scale with the very simple patterns that they form in map view.

The magnetic basalts or magnetic graywackes occur with interlayered nonmagnetic graywacke, and much rarer chert and limestone, are generally sheared, and may or may not be laterally continuous beyond the mapped localities. Basalt outcrops in the Fort Bragg area (Fig. 1, inset; Fig. 7), mapped as elongate bodies by Kramer (1976) based on projections between definite outcrops as much as 1 km apart, do suggest considerable lateral continuity along the magnetic anomalies, however, and most or even all of the anomalies there and to the north may be caused by magnetic basalt. We have no evidence for magnetic graywacke in the northern two thirds of the Coastal Belt. Magnetic graywacke is recognized in the southern part of the Coastal Belt, where it occurs as beds and

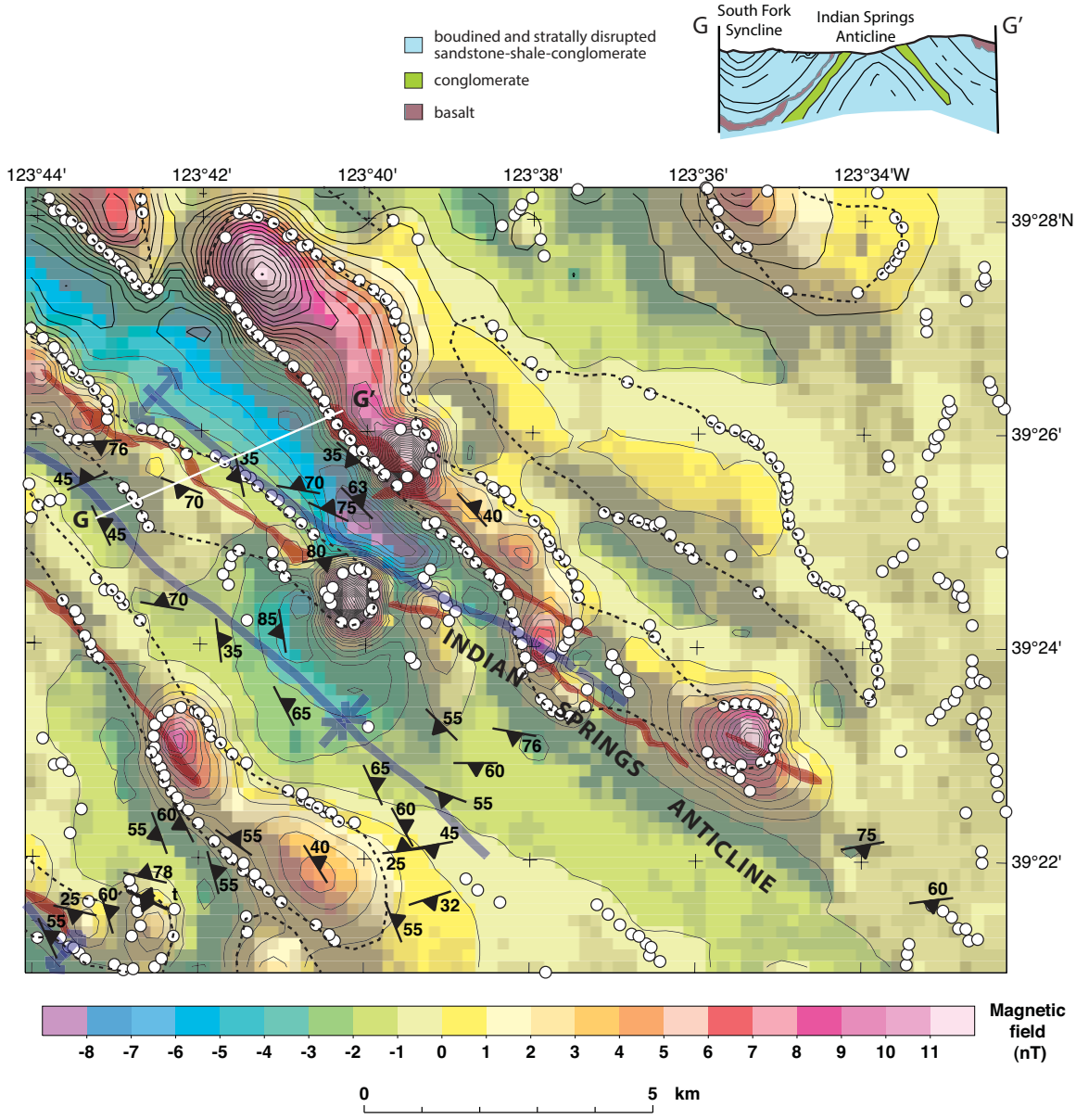

Figure 7. Filtered aeromagnetic map of Indian Springs anticline east of Fort Bragg and cross section G-G′ (white line) modified from Kramer (1976). Brown polygons, dark blue lines, and black symbols are basalt, fold axes, and shear fabric orientations, respectively, from Kramer (1976). White circles denote magnetization boundaries. Dotted lines outline extent of anomalies. Magnetic body associated with northeast limb of Indian Springs anticline has shallow to medium northeast dip based on magnetic anomaly asymmetry.

sheared pods interlayered with nonmagnetic graywacke at outcrop scale. Most of the anomalies here could be due to magnetic graywacke, although the southern basalt localities are also associated with magnetic anomalies, and both magnetic basalt and magnetic graywacke are associated with one anomaly at the south end of the Coastal Belt along the San Andreas fault (lavender anomaly in Fig. 6).

Because determining the detailed architecture of the magnetic layers within the Coastal Belt is difficult due to generally poor exposures, we examined a possible analog of the Coastal Belt volcanic-layer assemblage where the geology is better exposed. A stack of accreted south- to southwest-dipping thrust sheets (tabular bodies) composed variously of thin layers of oceanic pillow basalt overlain by Jurassic chert and/or graywacke of the Marin Headlands terrane of the Franciscan Complex (Central Belt) is exposed at the Marin Headlands just north of San Francisco (MH in Fig. 1; Fig. 8). Like the Coastal Belt volcanics, the Marin Headlands volcanics are strongly magnetic; the other rock types in this area are not. We processed the aeromagnetic data over the Marin Headlands in the same way we processed the Coastal Belt data, and the results are shown in Figure 8, together with a geologic map simplified from Wahrhaftig (1984).

The filtered magnetic anomalies over the Marin Headlands are quite similar to those over the Coastal Belt, and their relation to the detailed

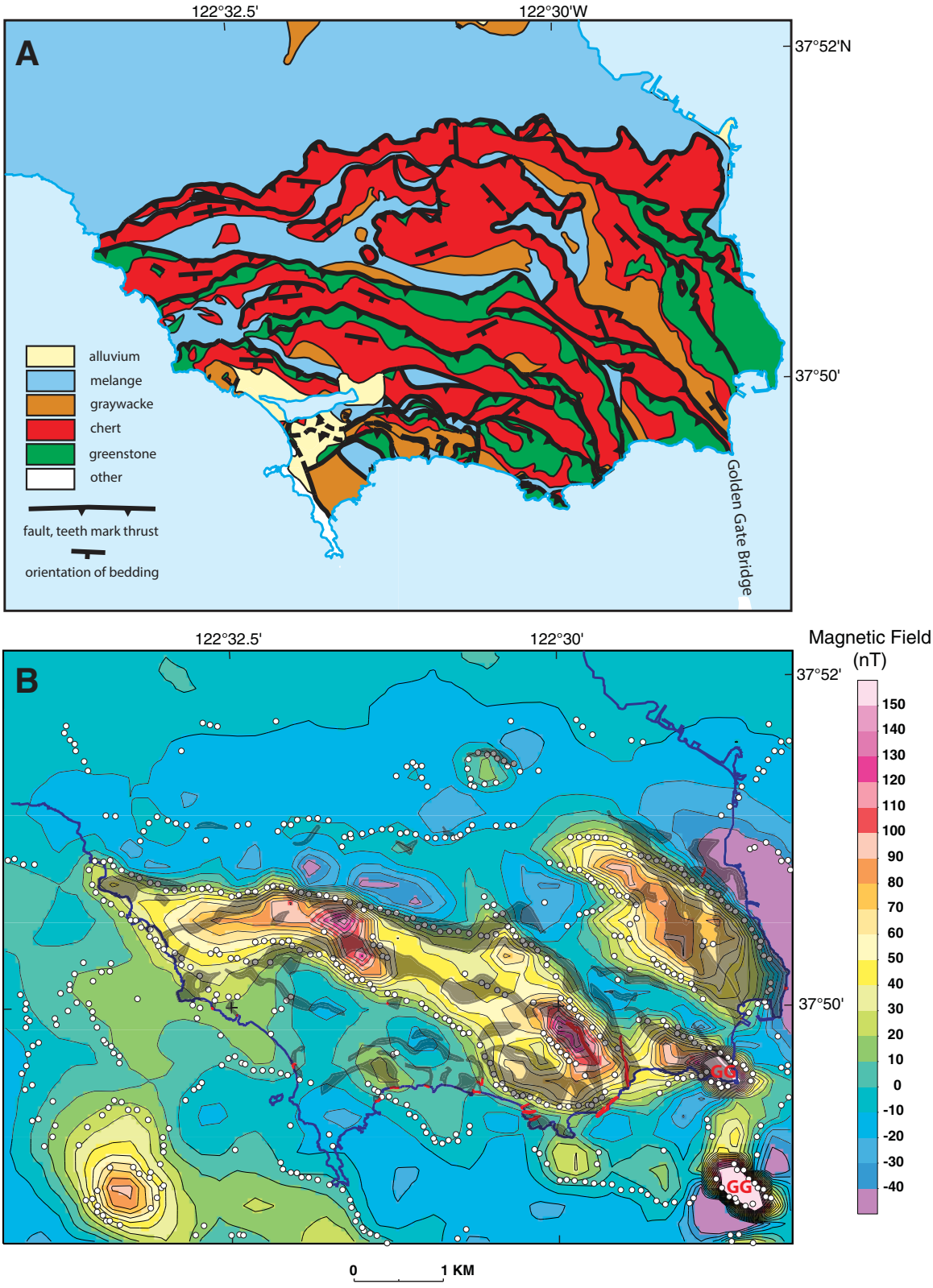

Figure 8. (A) Geologic and (B) filtered aeromagnetic maps of the Marin Headlands. Comparison of these two maps highlights how the magnetic data express a more generalized geometry of the imbricate slices of magnetic greenstone. Geology is modified from Wahrhaftig (1984). Magnetic data are from U.S. Geological Survey (1996). White circles—magnetization boundaries derived from filtered aeromagnetic data, gray transparent areas—outlines of greenstone, and GG—Golden Gate Bridge tower. Mélange (blue polygons in A) may also include more coherent rocks.

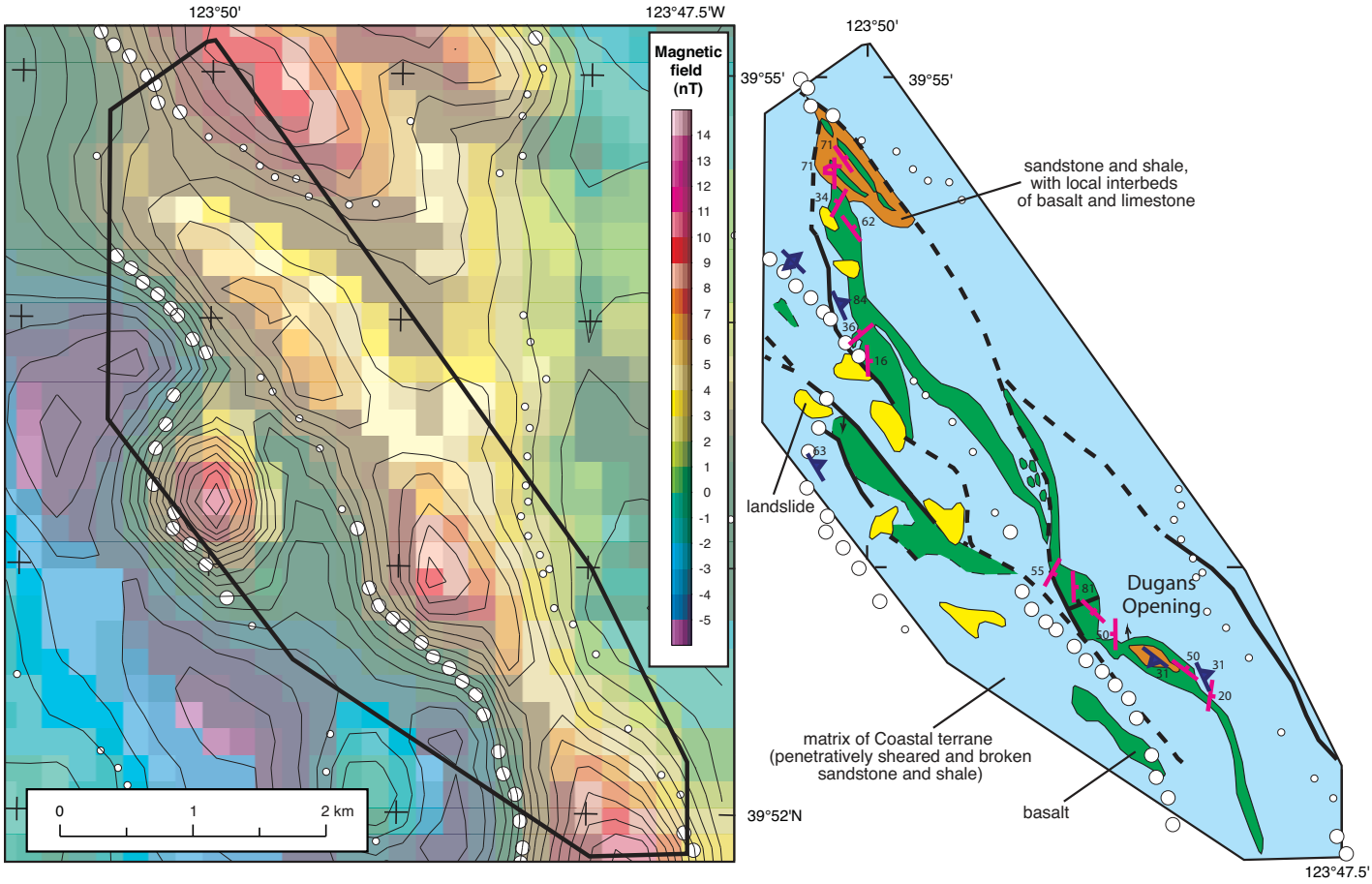

Figure 9. Filtered aeromagnetic map (left) modified slightly from Langenheim et al. (2011) and geologic map (right) modified from McLaughlin et al. (1994) of Dugans Opening area. White circles—magnetization boundaries. Magenta symbols—attitudes measured on sandstone and basalt; dark blue symbols—strike and dip of shear fabric. Magnetic high is parallel to and encompasses basalt bodies. Asymmetry of magnetic anomaly predicts moderate to steep dip to the northeast, whereas measured attitudes are more variable.

geology of the Marin Headlands provides potential insights into understanding the magnetic layer architecture in the Coastal Belt. The Marin Headlands basalts produce two major curvilinear anomalies approximately 1 km or less wide, 5–10 km long, and separated by roughly 2–3 km, with anomaly asymmetry indicating generally south- to southwest-dipping tabular bodies. Thus, these two anomalies have characteristics similar to those in the Coastal Belt. Comparison of the Marin Headlands anomalies with the geologic map indicates that the two anomalies are each produced by more than one magnetic basalt layer, with the southern anomaly apparently reflecting at least five mapped, structurally repeated basalt layers and their overlying chert and/or graywacke, some of which strike at an angle to the trend of the anomaly. Other basalt layers apparently are too thin or isolated to produce observable aeromagnetic anomalies.

The Marin Headlands example shows that multiple thin basalt layers (multiple tectonic slices of basalt basement) can produce a fairly simple single linear anomaly that results from smoothing of the magnetic field measured at the height of an airborne survey. This insight likely applies to the basalt source anomalies in the Coastal Belt, at least based on a limited number of detailed comparisons between the Coastal Belt geology and magnetic anomalies. These comparisons include (1) a single magnetic anomaly over at least two basalt layers near the east end of the Indian Springs anticline mapped by Kramer (1976) (Fig. 7), (2) multiple basalt layers beneath the magnetic anomaly at Dugans Opening mapped by McLaughlin et al. (1994) (Fig. 9), (3) multiple narrow magnetic anomalies and their associated inferred sources detected by a ground magnetic traverse beneath a single broader aeromagnetic anomaly at McKerricher State Park (Langenheim et al., 2011), 5 km north of Fort Bragg, and (4) the observation at McKerricher State Park that the magnetic basalt within a magnetic layer forming an anomaly hundreds of meters wide (at aircraft height) occurs in blocks with characteristic dimensions of meters to tens of meters, surrounded by nonmagnetic sandstone and limestone. The similarity in magnetic patterns throughout the Coastal Belt suggests that anomalies arising from magnetic graywacke also arise from multiple, narrow layers of magnetic graywacke surrounded by nonmagnetic sandstone and shale, but these are more difficult to map than the more distinctive basalt.

REGIONAL STRUCTURE

The plan pattern of the magnetic anomalies in the Coastal Belt (Fig. 1, inset; Fig. 2) and our conclusion that these represent tabular layers containing magnetic basalt and magnetic graywacke imply a rather simple structural organization, at least with respect to the magnetic layers themselves. The generally parallel pattern of the anomalies, the inferred locally opposed dips of the magnetic layers, and the local presence of U-shaped anomalies all suggest folding around subhorizontal to steeply plunging axes.

Regional differences in strike direction and local irregularities in trend suggest organization of the anomalies into domains (Fig. 6) separated by faults or zones of deformation.

Structural Domains from Anomaly Patterns

We used the anomaly patterns to define four structural domains (Fig. 6), and here we discuss the implied structure of the magnetic layers for each. Domain 1 is characterized by a group of long, northwesterly striking anomalies in the vicinity of Fort Bragg. These define at least seven, subparallel, northwest-trending layers, six of which have closely associated basalt localities, with some of those mapped bodies elongate along the trends of the layers (inset in Fig. 1; Kramer, 1976). Dip directions inferred from the anomaly profiles for the central three of these layers suggest a simple, antiform-synform pair ~40 km long with a wavelength of ~6 km (Fig. 6). The flanking anomalies could be used to extend this set of folds, although their pattern is not quite so regular and suggests faulting. Most simply, these anomalies could represent a single basalt-bearing sheet deformed into a set of fairly tight, subhorizontal-axis folds that has been locally faulted. This interpretation is supported by two-dimensional magnetic modeling (Fig. 5B) and by interpretation of the surface geology in both map view and in cross sections by Kramer (1976) (Fig. 7). The magnetic model (Fig. 5B) makes explicit the implication of the plan pattern, i.e., that the layers are truncated by the topographic surface. The original areal extent of the now-folded and faulted sheet, using a fold length of 40 km and amplitude similar to the wavelength as a minimum limit, would exceed 1000 km^2.

Domain 2, just to the north, is dominated by several long, linear magnetic anomalies that have generally more northerly trends than those of domain 1 and that in the southeastern part of the domain fan slightly outward to the south. The central, relatively high-amplitude anomaly of this group has two large associated basalt localities, and thus likely marks a basalt-bearing magnetic layer. The parallel flanking anomalies are weaker and have no associated mapped localities of basalt. These anomalies could also have basalt sources that lie some distance beneath the ground surface or are of smaller aggregate volume. The regular plan pattern and spacing of these anomalies are similar to those of domain 1, and the simplest interpretation would be northward continuation from that domain of a single folded basalt-bearing sheet. The available dips inferred from the anomaly profiles here do not support simple folding, however, but instead indicate that the several adjacent layers all dip to the northeast. This sequence of magnetic layers and intervening nonmagnetic rocks could represent a stack of several independent magnetic layers, a single sheet repeated by faulting, or a single sheet deformed into subhorizontal folds with overturned axial planes. Overturning the folds as they extend northward can accomplish continuity with domain 1 and seems the simplest interpretation. O'Day (1974) proposed an anticline-syncline pair with the same trend as the layers in domain 2, but the 10 km wavelength of his fold is about twice that suggested by the spacing of the magnetic anomalies. This discrepancy may be explained by the difficulty acknowledged by O'Day (1974) in mapping detailed structure limited to major streams and road cuts by thick soil and heavy vegetation, although many of his structural attitudes also indicate northeast dips.

The northern part of domain 2, beyond a small magnetically quiet gap, contains a set of short anomalies similar in trend to those to the south, with the eastern two apparently defining a slightly broken U-shaped pattern, open to the northwest. There is no continuity with the anomalies to the south, but folding on a similar trend and scale is possible.

The magnetic anomalies northeast of Punta Gorda form a different anomaly pattern that defines domain 3. Here, north of the westward-bending San Andreas fault at the Mendocino triple junction, the anomalies bend around fairly broad, east- to southeast-plunging folds (Fig. 1). These apparently follow folds expressed in the boundary between the False Cape terrane and overlying Coastal terrane, in non-Franciscan marine Miocene–Pliocene rocks, in the western boundary of the Yager terrane, and again in the folded Coastal Belt thrust. As in domains 1 and 2, the magnetic anomalies in the Coastal terrane here have several associated basalt localities, suggesting that these anomalies also represent basalt-bearing layers. In the Yager terrane, in contrast, the anomalies are in general weaker and are likely caused by magnetic sandstone and conglomerate (Langenheim et al., 2011).

The basalts of regions 1, 2, and 3 are considered to be remnants of old ocean floor and, where dated from associated limestones, are all latest Cretaceous in age (ca. 83–68 Ma; Sliter et al., 1986; inset in Fig. 1; Table 1). A plausible interpretation of most of the magnetic anomalies of domains 1, 2, and 3 is that they represent fragments from one piece of oceanic crust that have been incorporated into a single magnetic layer of remarkably constant thickness and then folded and otherwise deformed throughout the northern two thirds of the Coastal Belt. A single layer of this area may have been accreted in a short period of time, as has been suggested by Dumitru et al. (2013) based on the youngest detrital zircon ages from the Coastal Belt that cluster at 49–53 Ma.

South of domain 1, we assign the remainder of the Coastal Belt magnetic anomalies to domain 4, in which the pattern of anomalies is more variable than in the other domains. In contrast to the other domains, the source of the anomalies here is not principally basalt. Magnetic susceptibility measurements at various road cuts indicate that the source of many of the anomalies is magnetic graywacke (Phelps et al., 2008a, 2008b; Langenheim et al., 2011). Although this sampling is far from exhaustive, enough has been done to establish that graywacke sources dominate. Some basalt is also present, and we find direct evidence for both basalt and graywacke sources associated with a single magnetic anomaly (lavender anomaly in Fig. 6, located just east of and parallel to the San Andreas fault near Fort Ross; fig. 4 *in* Langenheim et al., 2011). The relation between the two source rocks is unknown, however, because they crop out on different traverses across the anomaly and because the area is highly sheared and heavily weathered.

Most striking in the varied anomaly patterns of domain 4 are the U-shaped anomalies in the northern part of the domain. The strong, northwest-opening U-shaped anomaly and the weaker ones immediately surrounding it north of Point Arena (green anomalies in Fig. 6; Langenheim et al., 2011), together with the associated dips, indicate a southeast-plunging antiform composed of at least two (possibly three) magnetic layers interleaved with nonmagnetic rock. The northeastern corner of the southeast-plunging antiform curves to the southwest and appears to be aligned with another U-shaped anomaly offset slightly eastward to the southeast (blue anomaly in Fig. 6). If this U-shaped anomaly, which opens southeastward, but lacks dip control to indicate the sense of folding, is connected to the northwest-opening U-shaped anomaly, it may represent a synform of Coastal Belt rocks. Although the U-shaped anomaly is located over mélange assigned to the Central Belt, the mélange is likely thin because it incorporates graywacke of the Coastal Belt. The southeastward-opening pattern thus suggests that folded magnetic Coastal Belt rocks extend beneath a thin flap of Central Belt rocks. These plunging folds are compatible as elements of a single regional deformation event that produced folds with wavelengths of 10–15 km, about twice the wavelength of the folding inferred from the magnetic anomalies in regions 1 and 2. In the southern part of domain 4, several sets of anomalies with different orientations suggest intervening faults, at least some of which could be related to faults that offset the Coastal Belt–Central Belt boundary.

The southern extent of domain 4 is difficult to define because of the complex structural relations between the Coastal Belt and Central Belt rocks. These complex relations make it difficult to distinguish anomalies produced by Coastal Belt rocks from those from Central Belt rocks. The magnetic anomaly produced by Eocene and Cretaceous basalt of the Wheatfield Fork terrane, for example, is almost overwhelmed by a larger magnetic anomaly associated with serpentinite along the highly modified Coastal Belt thrust. We have drawn the Coastal Belt thrust here using limited constraints from our reconnaissance geologic mapping, topography, and photogeologic interpretation. We have also included within the Coastal Belt most of the long, curvilinear anomalies that strike northwest at roughly the same trend as the major fold axes. We suspect that the sources of the long, curvilinear anomalies within the Central Belt that are parallel to Coastal Belt anomalies (Fig. 6) are concealed beneath a thin veneer of Central Belt mélange. Despite the added structural complexity in the southern part of domain 4, the wavelength of folding implied by the inliers of Central Belt is roughly equivalent to the rest of domain 4, although the wavelength appears to be shorter near the San Andreas fault.

We have delineated a small region within domain 4 at roughly latitude 38°45′N and bounded by the San Andreas fault to the southwest (Fig. 6): The short length and high amplitude of the anomalies in this region suggest that this region is different from the rest of domain 4, but we have not pursued the implications of this observation.

Boundaries between Structural Domains

The characteristics that we use to define the four structural domains, primarily strike direction, fold character, and magnetic sources, are easily recognizable, but the boundaries between the structural domains are more subtle. Domains 1 and 2 are differentiated primarily by a difference in anomaly strikes of 20°–30°, but the boundary region between the domains is less clearly defined. An abrupt discordance in anomaly strike between two anomalies definitely in separate domains occurs at the coast across a distance of ~2 km. In contrast, two of the prominent domain 1 anomalies farther offshore bend smoothly from the strike direction of domain 1 to that of domain 2 (Fig. 2), whereas 10–15 km to the east in the northern part of domain 1, two isolated anomalies have strike directions intermediate between those of domain 1 and domain 2. Thus, this boundary region seems to reflect a gradual transition between large regions with different fold orientations, perhaps accompanied by minor faulting, but it probably does not represent a major fault or shear zone with large offset.

Strike direction and complexity of anomaly pattern distinguish domain 2 from domain 3. The long, straight, north-northwest–trending anomalies of domain 2 contrast with the shorter, often strongly curved, more westerly trending anomalies of domain 3. The U-shaped (or broken U-shaped) anomalies in domain 3 suggest east-southeast–plunging folds, a suggestion supported by the similarly shaped boundaries between the Coastal terrane and the Yager terrane, the adjacent Coastal Belt thrust, and the antiformal exposure of the structurally lower False Cape terrane. In addition, the shape of the Coastal Belt thrust passes relatively smoothly between domains 2 and 3 with no major disruption. Thus, as with the boundary between domains 1 and 2, the boundary between domains 2 and 3 seems to reflect a gradual transition between areally extensive regions of different fold style, perhaps accompanied by minor faulting, but it does not seem to represent a major fault or shear zone with significant lateral offset.

The simplicity of the linear anomaly pattern in domain 1 contrasts with the more complex, curved, and cluttered pattern in adjacent domain 4 to the south. In addition, domain 4 includes, to the best of our knowledge, all the anomalies in the undivided Coastal Belt with magnetic graywacke sources. The boundary between domains 1 and 4 appears to be abrupt and marked by truncation of anomalies in domain 4. For these reasons, we suggest that this boundary could represent a fault, although it does not appear to significantly offset the Coastal Belt thrust.

We have defined four structural domains within the Coastal Belt based on trend, wavelength, and source of magnetic anomalies. The domains imply fairly distinct styles of folding and faulting. The boundaries between the domains 1, 2, and 3 are gradual, rather than abrupt, and thus do not indicate major faulting or shearing. The apparent absence of major faulting between these domains is supported by basalt being the only known source for the magnetic anomalies in domains 1, 2, and 3. Furthermore, it is plausible that the magnetic anomalies in these domains arise from a single folded layer of basalt. The boundary between domains 4 and 1, in contrast, could be a significant fault. Domain 4 also differs from the other domains in having graywacke as the dominant source of magnetic anomalies.

Age of Deformation

Constraints on the timing of the events that produced the structures expressed by the magnetic anomalies are few, although the structures must postdate the youngest deformed rocks. In domains 1, 2, and 4 (Fig. 6), those rocks are middle to late Eocene in age (Evitt and Pierce, 1975; Bachman, 1978; Sliter et al., 1984, 1986; McLaughlin et al., 1994; Blake et al., 2002). Overlying undeformed rocks in these domains are completely lacking, except between Fort Ross and Point Arena, where scattered patches of shallow-marine Ohlson Ranch Formation of Pliocene age (Fig. 1), which contains a ca. 4.4 Ma tuff (McLaughlin et al., 2012), unconformably overlie the Coastal Belt and its fault boundaries with northwest-trending bands of Central Belt rocks (Higgins, 1960; Peck, 1960; Blake et al., 2002). To the south, steeply dipping, northwest-trending reverse faults offset the late Miocene to late Pliocene Wilson Grove Formation (Fig. 1; Blake et al., 2002). The folding and faulting indicated by the magnetic anomalies in this part of the Coastal Belt are thus constrained to have occurred after the late Eocene and, at least south of Point Arena, before the middle to late Pliocene, although some younger movement on the northwest-trending faults is possible.

Rocks younger than Eocene are involved in the deformation that folded the magnetic layers in domain 3, which encompasses the Mendocino triple junction. The southeast-trending folds here prominently involve 18–22 Ma (Miocene) rocks of the False Cape terrane, as well as the older Coastal terrane–Yager terrane and Yager terrane–Central Belt boundaries to the east (Fig. 1). The folding of the magnetic layers here is thus at least as young as the early Miocene False Cape rocks. Even younger deformation is suggested by Pliocene and Miocene marine strata of Eel River basin affinity (Bear River beds of Ogle, 1953), which are caught up along the southwest flank of the False Cape terrane antiform, indicating continuation of folding at least into the Pliocene. Folds of similar orientation and wavelength deform Pliocene and late Pleistocene strata in the offshore and onshore parts of the Eel River forearc basin just to the north. This young compression seems to be associated with the present Mendocino triple junction, and the orientation of this folding does not appear to extend south into domain 2, where the magnetic anomalies are quite straight and trend north-northwest.

The fact that the Coastal Belt rocks south of domain 3 have not experienced folding similar to that of domain 3 is surprising, given that these rocks were adjacent to the Mendocino triple junction just a few million years ago (Atwater and Stock, 1998). This suggests that the present compressional regime producing west-northwest–trending faults and folds north of the triple junction is a relatively recent phenomenon, a conclusion that is supported by interpretations

of seismic-reflection data of the offshore Eel River basin (Clarke, 1992; Gulick and Meltzer, 2002) and studies of folded late Cenozoic strata onshore (McLaughlin et al., 1994, 2000; McCrory, 2000). The west-northwest orientation of folding in the vicinity of the triple junction differs from the predominant north-south orientation of folds and faults to the north along the Cascadia margin.

DISCUSSION AND IMPORTANT QUESTIONS DESERVING FURTHER STUDY

Origin of Layers

We have identified numerous magnetic anomalies that reflect thin, areally extensive layers distributed widely throughout the Coastal Belt and have used the magnetic signatures and inferred geometries of these layers to define a surprising, relatively simple regional structural organization that characterizes much of the Coastal Belt. Especially intriguing are questions about the origin and formation of these layers and what they may reveal about processes at an accretionary margin during and after accretion.

Any explanation of the origin of these layers should account for the following observations:

(1) The layers are relatively thin (a few hundred to perhaps 700 m thick).

(2) Individual layers may have an areal extent of more than 1000 km^2.

(3) In aggregate, the layers cover thousands of square kilometers.

(4) The magnetic source rocks are oceanic crustal basalts or lithic, volcanic-rich graywacke of arc origin.

(5) The magnetic layers are composed of rock bodies with characteristic dimensions of tens to perhaps a few hundred meters of intermixed magnetic and nonmagnetic materials.

(6) At least one layer contains both oceanic basalt fragments and lithic graywacke.

(7) The complexity and severity of deformation within a layer are considerably greater than the deformation of the layer boundaries, indicating that the layers are fault bounded.

A major question posed by the structures revealed by the magnetic data is why the magnetic structure is seemingly simpler than field relations in several areas would indicate. For example, in domain 3, the Yager and Coastal terranes of the Coastal Belt are clearly folded at several scales, with multiple generations of folding documented in the Yager terrane (McLaughlin et al., 1994). Outcrops in domain 4 along Fish Rock Road (latitude ~38°52′N, longitude 123°25′W) also exhibit a complex structure that contrasts with the continuity of relatively simple tabular magnetic sources over distances of tens of kilometers. Complexity at outcrop scale is not resolvable by the aeromagnetic data, which express a more generalized geometry of these fault-bounded, internally folded packages. The Marin Headlands comparison (Fig. 8) suggests that the airborne data may only be capable of resolving features that are wider or thicker than 100–200 m. An additional possibility is that the entire Coastal Belt consists of a stack of thin, widespread fault-bounded layers, only some of which can be recognized because they are magnetic. This style of faulting is suggested by seismic-reflection data interpreted as underplating at a range of depths within the Japanese subduction-zone complex (Bangs et al., 2004; Kimura et al., 2010).

The observation that the magnetic anomalies reflect fault-bounded, internally and complexly folded packages provides insight into the origin of these tectonic layers. Given that the Coastal Belt is an accretionary complex, these layers are presumed to be the result of accretion of the Coastal Belt at the continental margin. The narrow width (thickness) and great lateral extent of the magnetic layers (regardless of whether basalt or graywacke is the source), which span the four structural domains (Fig. 6), suggest a common process of generation. Rheological contrasts between more competent basalt and less competent, presumably fluid saturated graywacke and argillite have been proposed for generating fault and shear zones of up to 1 km thickness along a subduction megathrust (Fagereng and Sibson, 2010) and can explain generation of basalt layers. However, this mechanism does not explain generation of layers of magnetic and nonmagnetic graywacke, given that a contrast in magnetic property is not likely to be accompanied by a contrast in rheology. Debris scraped from the top of a large seamount consumed in a subduction zone could produce a widespread, thin layer of Cretaceous oceanic basalt scraps with associated limestone and chert, and engulfed in nonmagnetic graywacke, in the wake of the seamount (Ballance et al., 1989). Regular layering would be absent beneath the debris layer (i.e., behind the subducting seamount) however, and a completely different mechanism would be needed to account for the magnetic graywacke layers, even though they are geometrically similar to layers incorporating the oceanic basalt. Alteration that results in permeability and porosity changes in the upper 100–150 m of oceanic crust can explain thin, laterally widespread layers of basalt peeled up (and likely folded) into the accretionary complex (Kimura and Ludden, 1995). The depth at which this process is inferred to occur (4–6 km; Matsumura et al., 2003) is compatible with that inferred for the Coastal Belt (<5–8 km; Ernst and McLaughlin, 2012). It is not clear, however, how applicable this mechanism is for generating the fault-bounded layers of magnetic and nonmagnetic graywacke that reside in domain 4. Turbidity currents can generate laterally extensive beds of magnetic and nonmagnetic graywacke; however, they cannot generate simple tabular bodies that are internally and complexly deformed. The process of generating fault-bounded layers of magnetic and nonmagnetic graywacke is a subject that deserves further study.

Nature and Origin of Stress Field Causing Folding

Of the Coastal Belt folds defined in this study, those in domain 3 are most readily identified with a likely cause of the folding—the stress field associated with the Mendocino triple junction compression. The open, east-southeast– to southeast-trending folds of domain 3, clearly defined both by the geologic map and the magnetic anomalies, have axes that are perpendicular to the direction of maximum compressive stress, which trends 20°–30° more northerly than that expected to the north for the Cascadia subduction zone from the direction of plate convergence (McCrory, 2000; magenta arrow labeled GOR in Fig. 1). The pattern of the folding in this domain is suggestive of two main generations of folding, where the first fold orientation is more northerly in strike (such as that in domain 2), and the subsequent fold orientation was refolded in the stress field associated with the Mendocino triple junction.

Various mechanisms, such as westward movement of the Klamath–Sierra Nevada–Great Valley block and northward impingement of the San Andreas system (Williams et al., 2006) or crustal thickening and uplift postulated to result from viscous coupling of the southern edge of the Gorda plate to the base of the North American crust (Furlong and Govers, 1999), have been proposed to explain the source of triple junction compression. We prefer an alternate explanation for Mendocino triple junction compression that is produced by the collision of the North American plate against the buttress formed by the northern edge of the Pacific plate. The surface expression of this buttress is the trace of the Punta Gorda reach of the San Andreas fault, which is parallel to the fold axes in domain 3. Furthermore, the folds of domain 3 are confined to the region north of this reach. Thus, the location and orientation of domain 3 folds are consistent with compression across the Pacific plate buttress as the North American plate moves southeast relative to the Pacific plate along a trajectory that is more southerly than the Punta Gorda reach (Fig. 1), basically parallel to the Point Reyes–Point Arena reach of the San Andreas fault.

The North American plate has been moving southeast relative to the Pacific plate for many millions of years (Atwater and Stock, 1998), so domains 1, 2, and 4 must once have occupied a position relative to the northern edge of the Pacific plate similar to that of domain 3 today. Thus, it might seem puzzling that the fold styles and orientations within domains 1, 2, and 4 are so different from those of domain 3. We believe the explanation for the differences between the folds in domain 3 and the other Coastal Belt folds lies in the local plate interactions near the triple junction.

North of the Pacific plate buttress, the North American plate (and its included Coastal Belt rocks) extends farther to the west than the eastern corner of the Pacific plate, thus presenting a space problem associated with the passage of the westernmost North America around the eastern edge of the Pacific plate buttress. One way to accommodate this space problem is to have domain 3 rotate clockwise and compress transversely enough that it can slip past the eastern edge of the buttress. Such an accommodation would cause the fold axes to become more northerly and the folds to become somewhat tighter, much like we see in domain 2 to the south. In fact, clockwise bending of the major fold axes along the eastern margin of domain 3 (Fig. 1) and the tightening of the folds immediately south of domain 3 may reflect just such rotation and compression. Alternatively, the fold axes are bent by whatever process that creates the westward (or compressive) bend in the surface trace of the San Andreas fault.

Within the context of this proposed model for fold formation and evolution, the differing fold characteristics between domains 1 and 2, and between domains 1 and 4 could simply reflect changes in local interactions between the Pacific and North American plates at the times during which these transition zones were in the vicinity of the triple junction.

One other major contributor to the evolution of the folds in domains 1, 2, and 4 could possibly be the influence of the large releasing bend in the San Andreas fault between Point Arena and Point Delgada (Fig. 1). Southeast passage of the North American plate past the releasing bend would create an extensional environment along the western edge of the North American plate. One way to compensate for the extensional setting yet not leave a void along the San Andreas fault would be for the western edge of North America to smoothly collapse westward to fill the void. The major effect of such a collapse on existing folds would be a slight clockwise rotation (at most ~30° along the extreme western edge) of the axes of folds adjacent to the bend. Such a small rotation would be difficult to identify, but perhaps the slight southward fanning of the long magnetic anomalies in domain 2 reflects such a process. Alternatively, and perhaps more likely, southward fanning of these anomalies could be caused by accretion of the King Range terrane. These questions merit further study.

Implications of Folded Layer(s?) at Present Topographic Surface

Structural domains 1, 2, and 3 may reflect a single folded layer of basalt (itself internally and complexly folded and sheared) that resides within 2 km of the present-day erosion surface, although these rocks and enclosing clastic sedimentary rocks were once at maximum burial depths of 5–8 km (Ernst and McLaughlin, 2012). The apparent continuity and extent of the folded layer thus might suggest fairly spatially uniform long-term uplift and exhumation for much of the Coastal Belt, which is somewhat surprising given the passage of the Mendocino triple junction and models that predict significant uplift and exhumation (>1 km) produced by coupling of the southern edge of the Gorda plate with the overlying North American crust (Lock et al., 2006). A handful of fission-track dates indicate that most of the exhumation and cooling of the Coastal Belt took place in the period 10–20 Ma and may be reflected by a major angular unconformity that separates Coastal Belt rocks from overlying early middle Miocene sediments (Dumitru, 1989; Bachman et al., 1984; McLaughlin et al., 1982, 1994). Folding may have postdated (or accompanied later stages of) this period of uplift because of the similar style of folding of the Miocene overlap strata and the terrane boundaries. A maximum extent of 200 m of structural relief is suggested by faulting and tilting of the base of the Pliocene Ohlson Ranch Formation (Higgins, 1960; Lock et al., 2006). The interpretation that the magnetic anomalies of domains 1–3 reflect a single folded layer, if correct, may place constraints on the areal extent and timing of long-term uplift and exhumation that exceeds 2 km.

SUMMARY AND CONCLUSIONS

The Coastal Belt rocks record a major Franciscan accretionary episode along the northern California continental margin that over most of its latitudinal extent involved an Eocene sedimentary prism deposited on Late Cretaceous seafloor. In contrast to the earlier accreted Central and Eastern Belt rocks, the Coastal Belt rocks were carried no deeper than 5–8 km into the subduction zone, and thus are only mildly metamorphosed (Ernst and McLaughlin, 2012). Most of the rocks were deformed to broken formation and locally more severely. Continuing subduction and accretion to the north, near the Mendocino triple junction, involved Miocene and even Pliocene rocks. To the west, outboard accreted rocks of the Miocene False Cape terrane are raised in the core of an antiformal fold, one of several east- to southeast-trending folds near the triple junction that involve all the rocks and their fault boundaries from the False Cape terrane east to the westernmost Central Belt (Fig. 1).

Although the Coastal Belt is deformed at outcrop scale to broken formation with evident folds and faults, recently acquired aeromagnetic data reveal that the Coastal Belt is marked almost throughout by a set of tabular structural layers that are consistently thin (≤700 m) but of strike extent reaching 40 km and inferred unfolded areal extent greater than 1000 km^2. The observation of more severe deformation within the layers than that indicated by the map pattern of the layers requires that the layer boundaries are faults. We judge that the numerous parallel and in places clearly folded magnetic layers represent one or several original sheets, bounded by faults, that probably formed early in the accretionary process as subducting material was scraped off the downgoing slab and incorporated into the accreting prism. Those magnetic layers in the northern two thirds of the Coastal Belt could represent a single original structural layer that is magnetic because it contains fragments of basalt broken from the subducting oceanic crust. The origin of the layers farther south that contain magnetic graywacke rather than basalt is even less clear, but the similarity in layer dimensions seems to require a similar method of formation.

Once formed, these magnetic structural layers, and inferred nonmagnetic equivalents that form the balance of the rock mass, were deformed into folds with subhorizontal axes and relatively steep upright to overturned axial planes, limbs as long as 40 km, and wavelengths of several kilometers. The depth extent of these folds, inferred from their magnetic expressions, is no more than ~2 km. The folded magnetic layers thus occupy a zone ~2 km deep beneath the present erosion surface, which is surprising given the amount of uplift (>1 km) inferred to accompany the passage of the Mendocino triple junction.

Parallelism of anomalies and terrane boundaries indicates that the events that produced the folds in the Coastal Belt rocks occurred during or after the amalgamation of the Coastal and Yager terranes and after the Coastal Belt rocks were thrust beneath the Central Belt rocks along the Coastal Belt thrust. In the area of the triple junction, this relative timing is reflected in the corresponding curved shapes of the Coastal Belt thrust, the Coastal terrane–Yager terrane boundary, and the curved magnetic anomalies within

the Coastal terrane, which define an east-plunging antiform-synform pair with axes striking approximately east-west. Here, this deformation also involves rocks as young as late Pleistocene. In the southern third of the Coastal Belt, northwest-trending narrow fingers of Central Belt units that project into the Coastal Belt appear to be roughly associated with northwest-trending narrow folds within the Coastal Belt implied by the magnetic anomalies. The pattern is not as rigorous as that to the north, implying some decoupling between the Central and Coastal Belts and perhaps some later faulting. Coastal and Central Belt rocks and their bounding faults are locally overlain by relatively unfolded and unfaulted Pliocene deposits.

The plan pattern of the magnetic layers differs systematically across the map extent of the Coastal Belt, with several coherent areas of contrasting strike or pattern separated by relatively narrow transitional zones. Some appear to mark abrupt but continuous changes in strike, while others seem to mark fault zones. The structural organization revealed by the magnetic anomaly patterns not only raises questions about the timing and origin of these structures, but also provides a foundation for additional studies to answer these questions.

ACKNOWLEDGMENTS

This study would not have been possible without the support of the National Cooperative Geologic Mapping Program of the U.S. Geological Survey. We thank Russ Graymer and Ray Wells for their reviews of an earlier version of the manuscript. Reviews by Trevor Dumitru, an anonymous reviewer, and by Andrea Fildani improved the manuscript greatly. Dave Scholl provided encouragement and enthusiasm. Geoff Phelps and Jeana Lopez contributed many magnetic susceptibility measurements and stimulating discussion.

REFERENCES CITED

Aalto, K.R., McLaughlin, R.J., Carver, G.A., Barron, J.A., Sliter, W.V., and McDougall, K., 1995, Uplifted Neogene margin, southernmost Cascadia-Mendocino triple junction region, California: Tectonics, v. 14, p. 1104–1116, doi:10.1029/95TC01695.

Atwater, T., and Stock, J., 1998, Pacific–North America plate tectonics of the Neogene southwestern United States: An update: International Geology Review, v. 40, p. 375–402, doi:10.1080/00206819809465216.

Bachman, S.B., 1978, Cretaceous and Early Tertiary subduction complex, Mendocino coast, northern California, *in* Howell, D.G., and McDougall, K.A., ed., Mesozoic Paleogeography of the Western United States, Pacific Coast Paleogeography Symposium 2: Los Angeles, Pacific Section, Society of Economic Paleontologists and Mineralogists, p. 419–430.

Bachman, S.B., Underwood, M.B., and Menack, J.S., 1984, Cenozoic evolution of coastal northern California, *in* Crouch, J.K., and Bachman, S.B., eds., Tectonics and Sedimentation along the California Margin: Pacific Section, Society of Economic Paleontologists and Mineralogists Publication 38, p. 55–66.

Bailey, E.H., Irwin, W.P., and Jones, D.L., 1964, Franciscan and Related Rocks, and their Significance in the Geology of Western California: California Division of Mines and Geology Bulletin 183, 177 p.

Ballance, P.F., Scholl, D.W., Vallier, T.L., Stevenson, A.J., Ryan, H., and Herzer, R.H., 1989, Subduction of a Late Cretaceous seamount of the Louisville Ridge at the Tonga Trench: A model of normal and accelerated tectonic erosion: Tectonics, v. 8, p. 953–962, doi:10.1029/TC008i005p00953.

Bangs, N.L., Shipley, T.H., Gulick, S.P.S., Moore, G.F., Kuromoto, S., and Nakamura, Y., 2004, Evolution of the Nankai Trough décollement from the trench into the seismogenic zone: Inferences from three-dimensional seismic reflection profiling: Geology, v. 32, p. 273–276, doi:10.1130/G20211.2.

Blake, M.C., Jr., Jayko, A.S., McLaughlin, R.J., and Underwood, M.B., 1988, Metamorphic and tectonic evolution of the Franciscan Complex, northern California, *in* Ernst, W.G., ed., Metamorphism and Crustal Evolution of the Western United States (Rubey Volume 7): Englewood Cliffs, New Jersey, Prentice-Hall, p. 1035–1060.

Blake, M.C., Jr., Helley, E.J., Jayko, A.S., Jones, D.L., and Ohlin, H.N., 1992, Geologic Map of the Willows 1:100,000 Quadrangle, California: U.S. Geological Survey Open-File Report 92-271, scale 1:100,000.

Blake, M.C., Jr., Graymer, R.W., and Stamski, R.E., 2002, Geologic Map and Map Database of Western Sonoma, Northernmost Marin, and Southernmost Mendocino Counties, California: U.S. Geological Survey Miscellaneous Field Studies Map MF-2402, scale 1:100,000, 45 p.

Clarke, S.H., Jr., 1992, Geology of the Eel River basin and adjacent region: Implications for late Cenozoic tectonics of the southern Cascadia subduction zone and Mendocino triple junction: American Association of Petroleum Geologists Bulletin, v. 76, p. 199–224.

Dumitru, T.A., 1989, Constraints on uplift in the Franciscan subduction complex from apatite fission track analysis: Tectonics, v. 8, p. 197–220, doi:10.1029/TC008i002p00197.

Dumitru, T.A., Wakabayashi, John, Wright, J.E., and Wooden, J.L., 2010, Early Cretaceous transition from nonaccretionary behavior to strongly accretionary behavior within the Franciscan subduction complex: Tectonics, v. 29, 24 p., TC5001, doi:10.1029/2009TC002542.

Dumitru, T.A., Ernst, W.G., Wright, J.E., Wooden, J.L., Wells, R.E., Farmer, L.P., Adam, J.R., and Graham, S.A., 2013, Eocene extension in Idaho generated massive sediment floods into Franciscan trench and into Tyee, Great Valley and Green River basins: Geology, v. 41, p. 187–190.

Ernst, W.G., 2011, Accretion of the Franciscan Complex attending Jurassic–Cretaceous geotectonic development of northern and central California: Geological Society of America Bulletin, v. 123, p. 1667–1678, doi:10.1130/B30398.1.

Ernst, W.G., and McLaughlin, R.J., 2012, Mineral parageneses, regional architecture, and tectonic evolution of Franciscan metagraywackes, Cape Mendocino–Garberville–Covelo 30 by 60 quadrangles, northwest California: Tectonics, v. 31, 29 p., TC1001, doi:10.1029/2011TC002987.

Evitt, W.R., and Pierce, S.T., 1975, Early Tertiary ages from the Coastal Belt of the Franciscan Complex, northern California: Geology, v. 3, p. 433–436, doi:10.1130/0091-7613(1975)3<433:ETAFTC>2.0.CO;2.

Fagereng, Å., and Sibson, R.H., 2010, Mélange rheology and seismic style: Geology, v. 38, p. 751–754, doi:10.1130/G30868.1.

Finn, C., 1990, Geophysical constraints on Washington convergent margin structure: Journal of Geophysical Research, v. 95, p. 19,533–19,546, doi:10.1029/JB095iB12p19533.

Furlong, K.P., and Govers, R., 1999, Ephemeral crustal thickening at a triple junction: The Mendocino crustal conveyor: Geology, v. 27, p. 127–130, doi:10.1130/0091-7613(1999)027<0127:ECTAAT>2.3.CO;2.

Grantz, A., Zietz, I., and Andreasen, G.E., 1963, An Aeromagnetic Reconnaissance of the Cook Inlet Area, Alaska: U.S. Geological Survey Professional Paper 316-G, p. 117–134.

Grauch, V.J.S., and Cordell, L., 1987, Limitations of determining density or magnetic boundaries from the horizontal gradient of gravity or pseudogravity data: Geophysics, v. 52, no. 1, p. 118–121.

Gulick, S.P.S., and Meltzer, A.S., 2002, Effect of the northward-migrating Mendocino triple junction on the Eel River forearc basin, California: Structural evolution: Geological Society of America Bulletin, v. 114, p. 1505–1519, doi:10.1130/0016-7606(2002)114<1505:EOTNMM>2.0.CO;2.

Higgins, C.G., 1960, Ohlson Ranch Formation, Pliocene, northwestern Sonoma County, California: University of California Publications in Geological Sciences, v. 36, p. 199–231.

Hillhouse, J.W., and Jachens, R.C., 2005, Highly magnetic Upper Miocene sandstones of the San Francisco Bay area, California: Geochemistry Geophysics Geosystems, v. 6, doi:10.1029/2004GC000876.

Irwin, W.P., 1960, Geologic Reconnaissance of the Northern Coast Ranges and Klamath Mountains, California, with a Summary of the Mineral Resources: California Division of Mines Bulletin 179, 80 p., map scale 1:500,000.

Jayko, A.S., and Blake, M.C., Jr., 1984, Sedimentary petrology of graywacke of the Franciscan Complex in the northern San Francisco Bay area, California, *in* Blake, M.C., Jr., ed., Franciscan Geology of Northern California: Society of Economic Paleontologists and Mineralogists, Pacific Section Book Series 43, p. 121–132.

Jayko, A.S., Blake, M.C., McLaughlin, R.J., Ohlin, H.N., Ellen, S.D., and Kelsey, H.M., 1989, Reconnaissance Geologic Map of the Covelo 30- × 60-Minute Quadrangle, Northern California: U.S. Geological Survey Miscellaneous Field Studies Map MF-2001, scale 1:100,000.

Jennings, C.W., 1977, Geologic Map of California: California Division of Mines and Geology, Geologic Data Map Series 2, map scale 1:750,000.

Kimura, G., and Ludden, J., 1995, Peeling oceanic crust in subduction zones: Geology, v. 23, p. 217–220, doi:10.1130/0091-7613(1995)023<0217:POCISZ>2.3.CO;2.

Kimura, H., Takeda, T., Obara, K., and Kasahara, K., 2010, Seismic evidence from active underplating below the megathrust earthquake zone in Japan: Science, v. 329, p. 210–212, doi:10.1126/science.1187115.

Kramer, J.C., 1976, Geology and Tectonic Implications of the Coastal Belt Franciscan Fort Bragg–Willits area, Northern Coast Ranges, California [Ph.D. thesis]: Los Angeles, University of California, 128 p., 4 plates.

Langenheim, V.E., Hildenbrand, T.G., Jachens, R.C., Campbell, R.H., and Yerkes, R.F., 2006, Aeromagnetic Map with Geology of the Los Angeles 30′ by 60′ Quadrangle, Southern California: U.S. Geological Survey Scientific Investigations Map 2006-2950, available at http://pubs.usgs.gov/sim/2006/2950 (accessed June 2009).

Langenheim, V.E., Graymer, R.W., Jachens, R.C., McLaughlin, R.J., Wagner, D.L., and Sweetkind, D.S., 2010, Geophysical framework of the northern San Francisco Bay region, California: Geosphere, v. 6, p. 594–620, doi:10.1130/GES00510.1.

Langenheim, V.E., Jachens, R.C., Wentworth, C.M., and McLaughlin, R.J., 2011, Aeromagnetic and Aeromagnetic-Based Geologic Maps of the Coastal Belt, Franciscan Complex, Northern California: U.S. Geological Survey Scientific Investigations Map 3188, pamphlet 20 p., 3 sheets, various scales, and database, available at http://pubs.usgs.gov/sim/3188/ (accessed January 2013).

Lock, J., Kelsey, H., Furlong, K., and Woolace, A., 2006, Late Neogene and Quaternary landscape evolution of the northern California Coast Ranges: Evidence for Mendocino triple junction tectonics: Geological Society of America Bulletin, v. 118, p. 1232–1246, doi:10.1130/B25885.1.

Matsumura, M., Hashimoto, Y., Kimura, G., Ohmori-Ikehara, K., Enjohji, M., and Ikesawa, E., 2003, Depth of oceanic-crust underplating in a subduction zone: Inferences from fluid-inclusion analyses of crack-seal veins: Geology, v. 31, p. 1005–1008, doi:10.1130/G19885.1.

McCrory, P.A., 2000, Upper plate contraction north of the migrating Mendocino triple junction, northern California: Implications for partitioning of strain: Tectonics, v. 19, p. 1144–1160, doi:10.1029/1999TC001177.

McLaughlin, R.J., Kling, S.A., Poore, R.Z., McDougall, K., and Beutner, E.C., 1982, Post–middle Miocene accretion of Franciscan rocks, northwestern California: Geological Society of America Bulletin, v. 93, p. 595–605, doi:10.1130/0016-7606(1982)93<595:PMAOFR>2.0.CO;2.

McLaughlin, R.J., Blake, M.C., Jr., Griscom, An., Blome, C.D., and Murchey, B.L., 1988, Tectonics of formation, translation, and dispersal of the Coast Range ophiolite of California: Tectonics, v. 7, p. 1033–1056.

McLaughlin, R.J., Sliter, W.V., Frederiksen, N.O., Harbert, W.P., and McCulloch, D.S., 1994, Plate Motions

Recorded in Tectonostratigraphic Terranes of the Franciscan Complex and Evolution of the Mendocino Triple Junction, Northwestern California: U.S. Geological Survey Bulletin 1997, 60 p.

McLaughlin, R.J., Ellen, S.D., Blake, M.C., Jr., Jayko, A.S., Irwin, W.P., Aalto, K.R., Carver, G.A., Clarke, S.H., Barnes, J.B., Cecil, J.D., and Cyr, K.A., 2000, Geology of the Cape Mendocino, Eureka, Garberville, and Southwestern Part of the Hayfork 30 × 60 Minute Quadrangles and Adjacent Offshore Area, Northern California, with Digital Database: U.S. Geological Survey Miscellaneous Field Studies Map MF-2336, scale 1:137,000.

McLaughlin, R.J., Blake, M.C., Jr., Sliter, W.V., Wentworth, C.M., and Graymer, R.W., 2009, The Wheatfield Fork terrane: A remnant of Siletzia (?) in Franciscan Complex Coastal Belt of northern California: Geological Society of America Abstracts with Programs, v. 41, no. 7, p. 519.

McLaughlin, R.J., Vazquez, J.A., Fleck, R.J., DeLong, S., Sarna-Wojcicki, A., Wan, E., Powell, C., II, and Prentice, C.S., 2012, The ash of Ohlson Ranch: A well-dated stratigraphic marker for constraining deformation across the northern San Andreas fault: San Francisco, California, American Geophysical Union, 2012 Fall Meeting, abstract T21D-2603.

Murchey, B.L., and Jones, D.L., 1984, Age and significance of chert in the Franciscan Complex, Marin Headlands, California, *in* Blake, M.C., Jr., ed., Franciscan Geology of Northern California: Society of Economic Paleontologists and Mineralogists, Pacific Section Book Series 43, p. 23–30.

O'Day, M.S., 1974, The Structure and Petrology of the Mesozoic and Cenozoic Rocks of the Franciscan Complex, Leggett-Piercey Area, Northern California Coast [Ph.D. thesis]: Davis, California, University of California, 152 p., 3 plates.

Ogle, B.A., 1953, Geology of Eel River Valley Area, Humboldt County: California Division of Mines and Geology Bulletin 164, 128 p.

Peck, J.H., Jr., 1960, Paleontology and correlation of the Ohlson Ranch Formation: University of California Publications in Geological Sciences, v. 36, p. 233–241.

Phelps, G.A., McLaughlin, R.J., Jachens, R.C., and Wentworth, C.M., 2008a, Aeromagnetic signatures reveal stratigraphic and structural relations in the Franciscan Complex east of the San Andreas fault, northern California: Geological Society of America Abstracts with Programs, v. 40, no. 1, p. 53.

Phelps, G.A., McLaughlin, R.J., Jachens, R.C., and Wentworth, C.M., 2008b, Using high resolution aeromagnetic data to map pervasive folding in the lithologically indistinct Franciscan Coastal Belt [abs.]: Eos (Transactions of the American Geophysical Union), v. 89, no. 53, Fall Meeting supplement, abstract GP43B-0815.

Roberts, C.W., and Jachens, R.C., 1999, Preliminary Aeromagnetic Anomaly Map of California: U.S. Geological Survey Open-File Report 99-440, 14 p., available at http://geopubs.wr.usgs.gov/open-file/of99-440/ (accessed August 2011).

Roberts, C.W., Jachens, R.C., and Oliver, H.W., 1990, Isostatic Residual Gravity Map of California and Offshore Southern California: California Division of Mines and Geology Geologic Map 7, scale 1:750,000.

Saad, A.F., 1969, Magnetic properties of ultramafic rocks from Red Mountain, California: Geophysics, v. 34, p. 974–987, doi:10.1190/1.1440067.

Saltus, R.W., Blakely, R.J., Haeussler, P.J., and Wells, R.E., 2005, Utility of aeromagnetic studies for mapping of potentially active faults in two forearc basins: Puget Sound, Washington, and Cook Inlet, Alaska: Earth, Planets, and Space, v. 57, p. 781–793.

Sliter, W.V., 1984, Foraminifers from Cretaceous limestone of the Franciscan Complex, northern California, *in* Blake, M.C., Jr., ed., Franciscan Geology of Northern California: Society of Economic Paleontologists and Mineralogists, Pacific Section Book Series 43, p. 149–162.

Sliter, W.V., McLaughlin, R.J., Keller, G., and Evitt, W.R., 1986, Paleogene accretion of Upper Cretaceous oceanic limestone in northern California: Geology, v. 14, no. 4, p. 350–353.

Underwood, M.B., and Bachman, S.B., 1986, Sandstone petrofacies of the Yager complex and the Franciscan Coastal Belt, Paleogene of northern California: Geological Society of America Bulletin, v. 97, p. 809–817, doi:10.1130/0016-7606(1986)97<809:SPOTYC>2.0.CO;2.

U.S. Geological Survey, 1996, Aeromagnetic Map of the Central San Francisco Bay Area: U.S. Geological Survey Open-File Report 96-530, scale 1:100,000.

U.S. Geological Survey and California Geological Survey, 2006, Quaternary Fault and Fold Database for the United States: http//earthquakes.usgs.gov/regional/qfaults/ (accessed April 2006).

Wahrhaftig, C., 1984, Structure of the Marin Headlands block, California: A progress report, *in* Blake, M.C., Jr. ed., Franciscan Geology of Northern California: Society of Economic Paleontologists and Mineralogists, Pacific Section Book Series 43, p. 31–50.

Williams, T.B., Kelsey, H.M., and Freymuller, J.T., 2006, GPS-derived strain in northwestern California: Termination of the San Andreas fault system and convergence of the Sierra Nevada–Great Valley block contribute to southern Cascadia forearc contraction: Tectonophysics, v. 413, p. 171–184, doi:10.1016/j.tecto.2005.10.047.